



ARTICLE

# mRNA localization mediates maturation of cytoplasmic cilia in *Drosophila* spermatogenesis

Jaclyn M. Fingerhut<sup>1,2</sup>  and Yukiko M. Yamashita<sup>1,2,3,4</sup> 

**Cytoplasmic cilia, a specialized type of cilia in which the axoneme resides within the cytoplasm rather than within the ciliary compartment, are proposed to allow for the efficient assembly of very long cilia. Despite being found diversely in male gametes (e.g., *Plasmodium falciparum* microgametocytes and human and *Drosophila melanogaster* sperm), very little is known about cytoplasmic cilia assembly. Here, we show that a novel RNP granule containing the mRNAs for axonemal dynein motor proteins becomes highly polarized to the distal end of the cilia during cytoplasmic ciliogenesis in *Drosophila* sperm. This allows for the incorporation of these axonemal dyneins into the axoneme directly from the cytoplasm, possibly by localizing translation. We found that this RNP granule contains the proteins Reptin and Pontin, loss of which perturbs granule formation and prevents incorporation of the axonemal dyneins, leading to sterility. We propose that cytoplasmic cilia assembly requires the precise localization of mRNAs encoding key axonemal constituents, allowing these proteins to incorporate efficiently into the axoneme.**

## Introduction

Cilia are microtubule-based structures present on the surface of many cells. These specialized cellular compartments can be nonmotile primary cilia that largely function in signaling or motile cilia that can either move extracellular materials (e.g., lung multiciliated cells) or allow for cell motility (e.g., *Chlamydomonas reinhardtii* flagellum, sperm in many species; Ishikawa and Marshall, 2011). It is well established that most cilia are separated from the bulk cytoplasm (Fig. 1 A), which serves to concentrate signaling molecules for rapid response to extracellular signals received by the cilia, and that the ciliary gate at the base of the cilia forms a diffusion barrier through which molecules must be selectively transported (Reiter et al., 2012; Wheway et al., 2018). However, recent studies identified an additional type of cilia, called cytoplasmic cilia, in which the axoneme (the microtubule-based core of the cilia) is exposed to the cytoplasm (Fig. 1 A; Avidor-Reiss et al., 2017; Avidor-Reiss and Leroux, 2015; Dawson and House, 2010; Fawcett et al., 1970; Sinden et al., 1976; Tates, 1971; Tokuyasu, 1975). Cytoplasmic cilia are found in human and *Drosophila melanogaster* sperm as well as in *Plasmodium falciparum* and *Giardia intestinalis*. There are two proposed advantages to cytoplasmic cilia: (1) faster assembly, as the cell does not need to rely on ciliary transport mechanisms, allowing for the assembly of longer cilia; and (2) proximity to mitochondria for energy (Avidor-Reiss and Leroux, 2015; Sinden

et al., 2010). Despite being found across diverse taxa, very little is known about how cytoplasmic cilia are assembled and whether their assembly bears similarity to that of traditional compartmentalized cilia (Desai et al., 2018).

Cytoplasmic ciliogenesis has been proposed to occur in two stages (Fig. 1 A; Avidor-Reiss and Leroux, 2015). In the first stage, microtubules are polymerized in a small compartmentalized region, which is similar to canonical compartmentalized cilia, at the most distal end of the cilia (Gottardo et al., 2013; Tokuyasu, 1975). This region is gated by a transition zone (Caudron and Barral, 2009; Kwitny et al., 2010; Vieillard et al., 2016). This entire compartmentalized region, called the ciliary cap or the growing end, migrates away from the basal body, which is docked at the nuclear membrane (Basiri et al., 2014; Fawcett et al., 1970). The ciliary cap does not change in size as the cilia elongates. The continued polymerization of microtubules inside the ciliary cap displaces recently synthesized microtubules out of the compartmentalized region, exposing them to the cytoplasm (Fig. 1 A). The second stage is axoneme maturation, in which additional axonemal proteins (e.g., axonemal dyneins, the motor proteins that confer motility by allowing axonemal microtubules to slide against each other; Fig. 1 B), are added to the bare microtubule structure after it emerges from the ciliary cap (Tates, 1971; Tokuyasu, 1975). Axoneme

<sup>1</sup>Cellular and Molecular Biology Program, University of Michigan, Ann Arbor, MI; <sup>2</sup>Life Sciences Institute, University of Michigan, Ann Arbor, MI; <sup>3</sup>Department of Cell and Developmental Biology, University of Michigan, Ann Arbor, MI; <sup>4</sup>Howard Hughes Medical Institute, University of Michigan, Ann Arbor, MI.

Correspondence to Jaclyn M. Fingerhut: [jaclynmf@umich.edu](mailto:jaclynmf@umich.edu); Yukiko M. Yamashita: [yukikomy@umich.edu](mailto:yukikomy@umich.edu).

© 2020 Fingerhut and Yamashita. This article is distributed under the terms of an Attribution–Noncommercial–Share Alike–No Mirror Sites license for the first six months after the publication date (see <http://www.rupress.org/terms/>). After six months it is available under a Creative Commons License (Attribution–Noncommercial–Share Alike 4.0 International license, as described at <https://creativecommons.org/licenses/by-nc-sa/4.0/>).

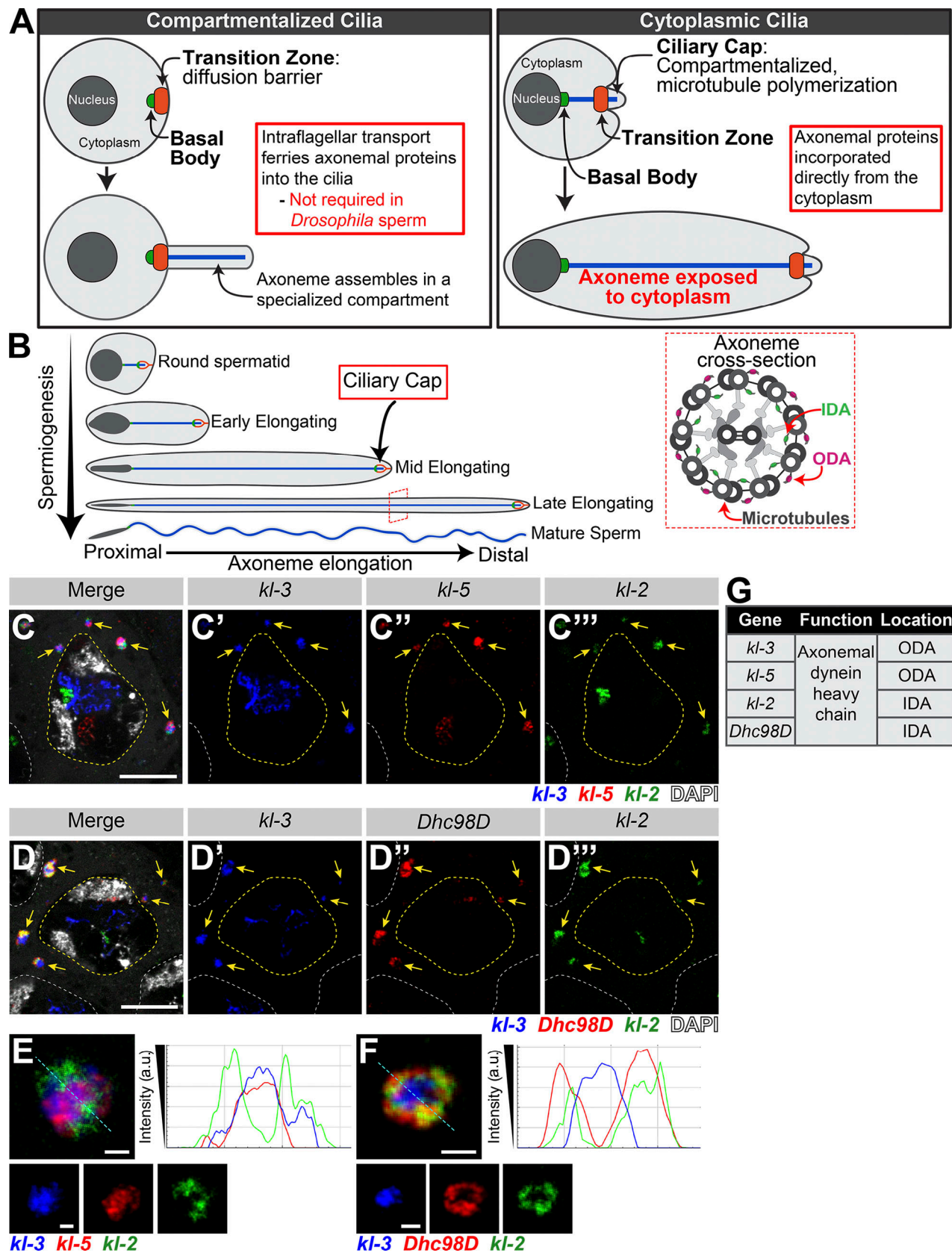


Figure 1. **Axonemal dynein heavy chain mRNAs colocalize in an RNP granule in SCs.** (A) Diagram comparing and contrasting traditional compartmentalized cilia and cytoplasmic cilia. Shown are the nucleus (dark gray), cytoplasm (light gray), basal body (green), transition zone (orange), and axoneme (blue). (B) Diagram of *Drosophila* spermiogenesis with stages of spermatid elongation. Shown are the nucleus (dark gray), cytoplasm (light gray), transition zone (green), ciliary cap (orange), and axoneme (blue). Axoneme cross-section image showing location of axonemal dynein arms. Shown are the microtubules and

other structural components (gray), IDA (green), and ODA (magenta). **(C and D)** smFISH against axonemal dynein heavy chain transcripts in SCs showing *kl-3*, *kl-5*, and *kl-2* mRNAs (C) or *kl-3*, *kl-2*, and *Dhc98D* mRNAs (D) in kl-granules. Shown are *kl-3* (blue), *kl-2* (green), *kl-5* (red, C), *Dhc98D* (red, D), DAPI (white), kl-granules (yellow arrows), SC nuclei (yellow dashed line), neighboring SC nuclei (white dashed line). Scale bars: 10  $\mu$ m. **(E and F)** smFISH against *kl-3*, *kl-5*, and *kl-2* (E) or *kl-3*, *kl-2*, and *Dhc98D* (F) showing a single kl-granule. Shown are *kl-3* (blue), *kl-2* (green), *kl-5* (red; E), *Dhc98D* (red; F). Intensity plots are shown for the regions marked by the cyan dashed line. Scale bars: 1  $\mu$ m. **(G)** Table listing the genes focused on in this study, their function, and their localization within the axoneme.

maturation was inferred to occur in the cytoplasm based on the dispensability of ciliary transport mechanisms and the inefficiency of relaying on diffusion through the transition zone (Avidor-Reiss and Leroux, 2015; Avidor-Reiss et al., 2004; Breslow et al., 2013; Briggs et al., 2004; Han et al., 2003; Hoeng et al., 2008; Kee et al., 2012; Lin et al., 2013; Sarpal et al., 2003). However, how this maturation process occurs in the cytoplasmic compartment to allow for cytoplasmic cilia formation remains unknown.

*Drosophila* spermatogenesis provides an excellent model for the study of cytoplasmic ciliogenesis (Fig. 1 B), owing to rich cytological knowledge of spermatogenesis and the conservation of almost all known ciliary proteins (Zur Lage et al., 2019). Developing spermatids elongate from 15  $\mu$ m to 1,900  $\mu$ m (1.9 mm; Bates, 1971; Tokuyasu, 1975). Within mature sperm, the cytoplasmic cilia are 1,800  $\mu$ m, and the ciliary caps (the compartmentalized region) are only  $\sim$ 2  $\mu$ m. Ciliogenesis starts in premeiotic spermatocytes (SCs), which assemble short primary (compartmentalized) cilia (Fabian and Brill, 2012; Gottardo et al., 2013; Riparbelli et al., 2012; Bates, 1971). Prior to axoneme elongation, these primary cilia, which were docked at the plasma membrane in SCs, invaginate, forming the ciliary cap. During axoneme elongation, the majority of the length of the cilia will be exposed to the cytoplasm, as described above. Accordingly, axoneme assembly in *Drosophila* does not require intraflagellar transport (IFT; Han et al., 2003; Sarpal et al., 2003), the process used by traditional compartmentalized cilia to ferry axonemal proteins from the cytoplasm into the ciliary compartment for incorporation (Rosenbaum and Witman, 2002). Other cytoplasmic cilia have been found not to require IFT for their assembly (Avidor-Reiss and Leroux, 2015; Briggs et al., 2004; Hoeng et al., 2008), leading to the appreciation of a distinct type of cilia; based on the dispensability of IFT, it was postulated that axoneme maturation must occur in the cytoplasm, hence the term cytoplasmic cilia.

It has long been known that SCs transcribe almost all genes whose protein products are needed postmeiotically and that these mRNAs may not be translated until days later when proteins are needed (Barckmann et al., 2013; Olivieri and Olivieri, 1965). We previously showed that the Y-linked testis-specific axonemal dynein heavy chain genes *kl-3* and *kl-5*, as well as the testis-specific axonemal dynein intermediate chain *Dic61B*, are transcribed in SCs (Fingerhut et al., 2019). However, axoneme elongation does not begin until after meiosis, suggesting that these mRNAs may not be translated until later in development. Intriguingly, we previously showed that *kl-3* and *kl-5* mRNAs localize to cytoplasmic granules in SCs. RNP granules (e.g., stress granules, P granules, and germ granules) are known to play critical roles in mRNA regulation, such as mediating the

subcellular localization of mRNAs and controlling the timing of translation (Anderson and Kedersha, 2009; Buchan, 2014; Medioni et al., 2012). Therefore, we decided to investigate the role of this novel RNA granule in the mRNA regulatory mechanisms that ensure proper axoneme assembly and found that it plays an essential role in mediating the incorporation of axonemal proteins, providing the first insights into the molecular mechanism of cytoplasmic cilia maturation. We show four axonemal dynein heavy chain mRNAs, including *kl-3* and *kl-5*, colocalize in these novel granules in late SCs along with the AAA+ (ATPases associated with diverse cellular activities) proteins Reptin (Rept) and Pontin (Pont). These RNP granules are segregated during the meiotic divisions and localize to the distal end of the cytoplasmic compartment as the axoneme elongates during spermiogenesis. We further show that Rept and Pont are required for RNP granule formation and that RNP granule formation is necessary for accumulation and incorporation of the axonemal dynein proteins into the axoneme. Our data suggest that cytoplasmic cilia maturation relies on the local translation of axonemal components such that they can be incorporated into the bare microtubule structure as it emerges from the ciliary cap.

## Results

### Axonemal dynein heavy chain mRNAs colocalize in RNP granules in SCs

In our previous study, we analyzed the expression of the Y-linked axonemal dynein genes *kl-3* and *kl-5* and showed that these two mRNAs localized to cytoplasmic granules in late SCs (Fingerhut et al., 2019). Using single-molecule RNA FISH (smFISH), we found that mRNAs for four testis-specific axonemal dynein heavy chain genes (the Y-chromosome genes *kl-2*, *kl-3*, and *kl-5*, as well as the autosomal gene *Dhc98D*; Carvalho et al., 2000; Goldstein et al., 1982; Hardy et al., 1981; Zur Lage et al., 2019) colocalize in RNP granules in the cytoplasm of late SCs, with each SC containing several of these cytoplasmic granules (Fig. 1, C and D). We termed these granules “kl-granules” after the three Y-linked constituent mRNAs. It should be noted that robust transcription of these genes is still ongoing in SC nuclei (visible as bright nuclear signal; Fig. 1, C and D) but these are nascent transcripts that still contain intronic RNA, whereas the kl-granules in the cytoplasm do not contain intronic RNA, as we showed previously (Fingerhut et al., 2019). The present study focuses on the fate of these cytoplasmic RNPs. mRNAs within a kl-granule appear spatially suborganized: *kl-3* and *kl-5* mRNAs, which encode outer dynein arm (ODA) dynein heavy chain proteins, cluster together in the core of the kl-granule while *kl-2* and *Dhc98D* mRNAs, which encode inner dynein arm (IDA)



dynein heavy chain proteins, localize peripherally (Fig. 1, E–G). This is similar to the subcompartmentalization observed in other RNP granules, including the germ granules in the *Drosophila* ovary, stress granules, P granules, nucleoli, and the dynein axonemal particles in human and *Xenopus* multiciliated cells (Boisvert et al., 2007; Jain et al., 2016; Lee et al., 2020a Preprint; Little et al., 2015; Trcek et al., 2015; Wang et al., 2014). We noted that kl-granule formation is unlikely to be dependent upon any one mRNA constituent, as RNAi-mediated knockdown of *kl-3*, *kl-5*, *kl-2*, or *Dhc98D* (*bam-gal4>UAS-kl-3<sup>TRIP.HMC03546</sup>* or *bam-gal4>UAS-kl-5<sup>TRIP.HMC03747</sup>* or *bam-gal4>UAS-kl-2<sup>GC8807</sup>* or *bam-gal4>UAS-Dhc98D<sup>TRIP.HMC06494</sup>*) did not perturb granule formation despite efficient knockdown (Fig. S1).

We conclude that mRNAs for the testis-specific axonemal dynein heavy chains localize to novel RNP granules, which we termed kl-granules, in late SCs.

### kl-granules segregate during meiotic divisions and localize to the distal end of elongating spermatids

As kl-granules contain mRNAs for axonemal proteins that are only necessary for spermiogenesis, we next followed the fate of the kl-granules through meiosis and into spermiogenesis. kl-granules segregate through the two sequential meiotic divisions (Fig. 2 A) such that each resulting haploid spermatid receives a relatively equal amount of kl-granule (Fig. 2 B). Upon completion of meiosis, the resultant spermatids are interconnected due to incomplete cytokinesis during the four mitotic divisions that occur early in germ cell development and the two meiotic divisions, forming a cyst of 64 spermatids (Fuller, 1993; Hime et al., 1996). As the axoneme starts to elongate within each spermatid, the nuclei cluster to the proximal end of the cyst while the axoneme elongates unidirectionally away from the nuclei with the ciliary caps clustered at the distal end of the cyst (Fig. 1 B; Fabian and Brill, 2012). Strikingly, we found that kl-granules become localized to the distal end of elongating spermatid cysts (Fig. 2 C). This polarized localization remains as the axoneme continues to elongate (Fig. 2, D and E). At later stages of elongation, kl-granules begin to dissociate and mRNAs become more diffusely localized at the distal end (Fig. 2, D and E). Interestingly, *kl-3* and *kl-5* mRNAs (encoding ODA proteins) separate from *kl-2* and *Dhc98D* mRNAs (encoding IDA proteins; Fig. 2, D and F). It is of note that this separation pattern correlates with the subgranule localization of constituent mRNAs described above (*kl-3* and *kl-5* localize to the core of the kl-granules [Fig. 1 E] whereas *kl-2* and *Dhc98D* localize to the periphery of the kl-granules [Fig. 1 F]) and was observed in 100% of elongating spermatid cysts ( $n = 269$ ).

These results show that kl-granules exhibit stereotypical localization to the growing end of spermatids after being segregated during meiosis, implying that programmed positioning of kl-granules may play an important role during spermatid elongation and axoneme maturation.

### The AAA+ proteins Rept and Pont colocalize with kl-granules

To further understand how kl-granules form and their potential function, we sought to identify a protein that localizes to kl-granules. In our previous study, we screened for proteins

involved in the expression of the Y-linked axonemal dynein genes (Fingerhut et al., 2019). Rept and Pont, two AAA+ proteins (Puchades et al., 2020), were included in this screen because of their high expression in the testis and their involvement in RNP complex formation in other systems (Mao and Houry, 2017; Robinson et al., 2013). Also, studies in *Drosophila*, mouse, zebrafish, *Chlamydomonas*, and *Xenopus* have specifically implicated Rept and Pont in axoneme/motile cilia assembly and/or sperm motility, although the underlying mechanism remains unknown (Dafinger et al., 2018; Huizar et al., 2018; Li et al., 2017; Stolc et al., 2005; Tammana and Tammana, 2017; Zhao et al., 2013; Zur Lage et al., 2018).

We found that Rept and Pont colocalize in cytoplasmic granules from the SC stage through elongating spermatids (Fig. 3, A and B). Immunofluorescent staining combined with smFISH showed that Rept and Pont colocalize with kl-granules. Pont first colocalizes with *Dhc98D* mRNA in early SCs (Fig. 3 C) and with all other kl-granule constituent mRNAs in later SCs (Fig. 3 D) and throughout spermatid elongation (Fig. 3 E). Close examination of kl-granules in late SCs revealed that Pont is not evenly distributed within a kl-granule and rather concentrates near the core with *kl-3* and *kl-5* mRNAs (Figs. 1 E and 3 F). In contrast, *kl-2* and *Dhc98D* mRNAs occupy the periphery of the kl-granule (Fig. 1 F), where Pont is less concentrated.

We conclude that Rept and Pont localize to kl-granules together with axonemal dynein heavy chain mRNAs. It is interesting to note that previous studies have proposed that Rept and Pont function as chaperones in the assembly of axonemal dynein motors (complexes containing a combination of dynein heavy, intermediate, and light chains; Huizar et al., 2018; Li et al., 2017; Zur Lage et al., 2018). However, the role of mRNA in the previously reported Rept- and Pont-containing chaperon complexes remains unexplored. Interestingly, a recent study reported the presence of RNA in this chaperon complex (although the identity of the RNAs remains unknown), raising the possibility that mRNA localization may be a universal mechanism (Drew et al., 2020 Preprint; see Discussion).

### Rept and Pont are required for kl-granule assembly

To explore the function of Rept and Pont in kl-granule formation, we performed RNAi-mediated knockdown of either *rept* or *pont* (*bam-gal4>UAS-rept<sup>KK105732</sup>* or *bam-gal4>UAS-pont<sup>KK101103</sup>*). In addition to eliminating the targeted protein, depletion of *rept* resulted in loss of Pont and vice versa, reminiscent of findings from previous studies, likely because these proteins stabilize each other as components of the same complex (Fig. S2; Gorynia et al., 2011; Li et al., 2017; Rivera-Calzada et al., 2017; Venteicher et al., 2008).

We next determined whether Rept and Pont are needed for kl-granule assembly. Indeed, knockdown of *rept* or *pont* resulted in disruption of kl-granules. smFISH clearly detected the presence of dispersed *kl-3* and *kl-5* mRNAs in late SCs, suggesting that *rept* and *pont* are required for kl-granule formation (Fig. 4, A–C; note that nuclear signal was oversaturated in order to focus on the dispersed cytoplasmic signal). This effect was more pronounced in elongating spermatids where *kl-3* and *kl-5* mRNAs were diffuse throughout the entire cyst in the RNAi

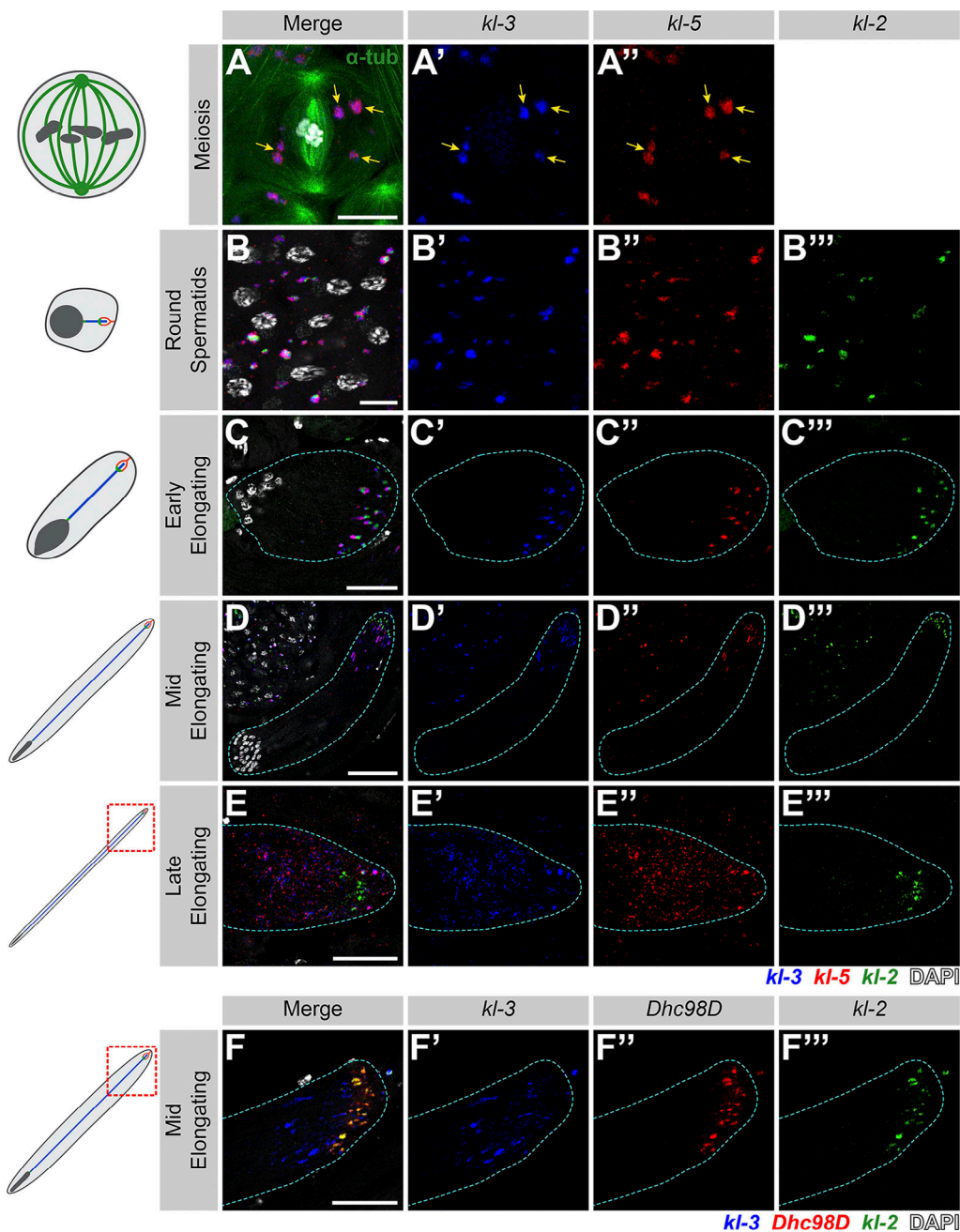
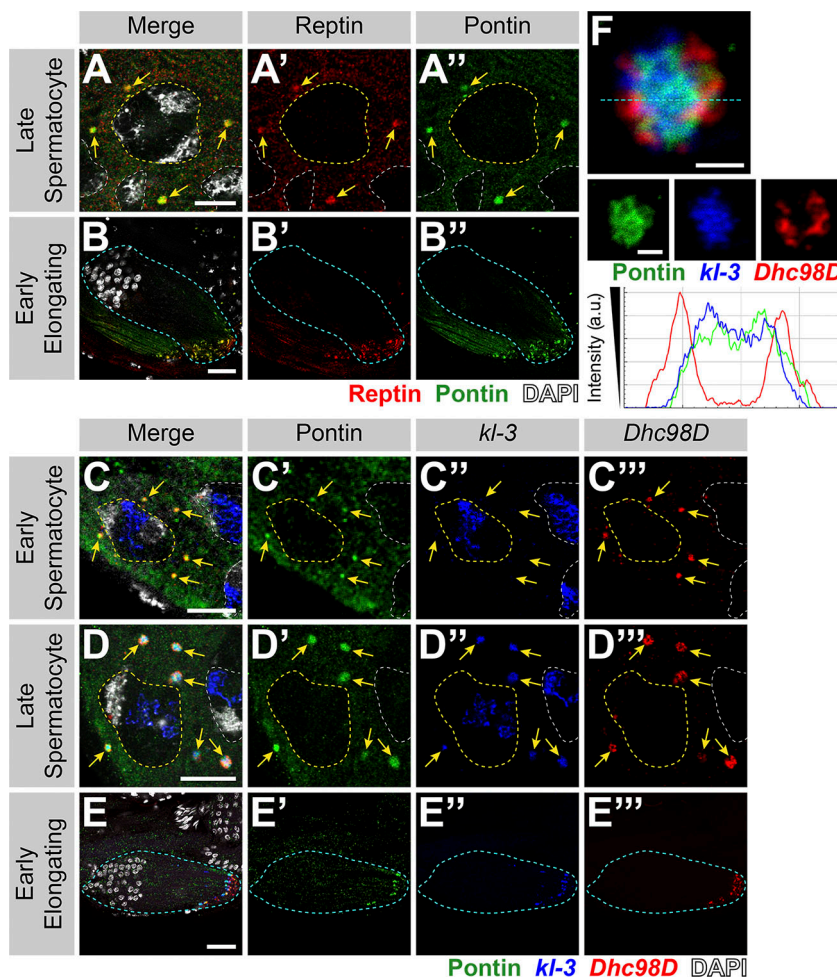


Figure 2. **kl-granules segregate during the meiotic divisions and localize to the distal end of elongating spermatids.** (A) smFISH against *kl-3* and *kl-5* during meiosis. Shown are *kl-3* (blue), *kl-5* (red),  $\alpha$ -tubulin-GFP (green), DAPI (white), and *kl*-granules (yellow arrows). Scale bar: 10  $\mu$ m. (B–E) smFISH against *kl-3*, *kl-5*, and *kl-2* during spermiogenesis. The round spermatid (B), early elongating spermatid (C), mid elongating spermatid (D), and late elongating spermatid (E) stages are shown. Shown are *kl-3* (blue), *kl-5* (red), *kl-2* (green), DAPI (white), and a spermatid cyst (cyan dashed line). Scale bars: 10  $\mu$ m (B), 25  $\mu$ m (C and E), or 50  $\mu$ m (D). (F) smFISH against *kl-3*, *Dhc98D*, and *kl-2* in mid elongating spermatids. *kl-3* (blue), *Dhc98D* (red), *kl-2* (green), DAPI (white), spermatid cyst (cyan dashed line). Scale bar: 25  $\mu$ m.

conditions (Fig. 4, D–F). Quantitative RT-PCR further demonstrated that mRNA levels were not reduced compared with cross-sibling controls (Fig. 4, G and H), demonstrating that *kl*-granule formation is not required for mRNA stability. This is in accordance with observations in other systems, which suggest that RNA granule formation is not required for mRNA stability and may be more important for mRNA localization or translation (Bley et al., 2015; Lee et al., 2020b).

Interestingly, knockdown of *rept* or *pont* had a somewhat different effect on *kl-2* and *Dhc98D* mRNAs. smFISH for *kl-2* and *Dhc98D* following RNAi of either *rept* or *pont* showed loss of *kl*-granule localization in late SCs similar to that seen for *kl-3* and *kl-5* (Fig. 4, I–K). However, in elongating spermatids, *kl-2* and *Dhc98D* mRNAs appeared to localize properly at the distal end of the cyst (Fig. 4, L–N). Considering that *Pont* primarily colocalized with *kl-3* and *kl-5* mRNAs (Fig. 3 F), this may suggest that



**Figure 3. Rept and Pont colocalize with kl-granules.** (A and B) Rept and Pont colocalization in SCs (A) and early elongating spermatids (B). Shown are Rept (red), Pont (green), DAPI (white), SC nuclei (yellow dashed line, A), neighboring SC nuclei (white dashed line; A), kl-granules (yellow arrows; C), and a spermatid cyst (cyan dashed line; B). Scale bars: 10  $\mu$ m (A) or 25  $\mu$ m (B). (C-E) Immunofluorescent staining combined with smFISH for Pont protein and *kl-3* and *Dhc98D* mRNAs in early SCs (C), late SCs (D), and early elongating spermatids (E). Shown are Pont (green), *kl-3* (blue), *Dhc98D* (red), DAPI (white), SC nuclei (yellow dashed line; C and D), neighboring SC nuclei (white dashed line; C and D), kl-granules (yellow arrows; C and D), and a spermatid cyst (cyan dashed line; E). Bar: 10  $\mu$ m (C and D) or 25  $\mu$ m (E). (F) Immunofluorescent staining combined with smFISH for Pont protein and *kl-3* and *Dhc98D* mRNAs in a single kl-granule. Pont (green), *kl-3* (blue), and *Dhc98D* (red). Intensity plot is shown for the region marked by the cyan dashed line. Scale bar: 1  $\mu$ m.

other proteins play a role in kl-granule formation or that there may be a differential requirement for these proteins between different mRNAs and over developmental time.

In conclusion, Rept and Pont are critical for assembling kl-granules.

#### kl-granule assembly is required for efficient Kl-3 translation and sperm motility

Previous studies in *Drosophila* and mouse demonstrated that Rept and Pont are required for male fertility (Li et al., 2017; Zur Lage et al., 2018). We confirmed that seminal vesicles, where mature motile sperm are stored after exiting the testis, were empty in *rept* or *pont* RNAi testes (Fig. 5, A-C), as was observed for *kl-3*, *kl-5*, *kl-2*, or *Dhc98D* RNAi testes (Fig. S3; Fingerhut et al., 2019; Zur Lage et al., 2018).

We further characterized the sterility phenotype of *rept* and *pont* RNAi testes and found that spermiogenesis fails during individualization. As sperm develop as cysts, the process of individualization removes excess cytoplasm from the spermatids and separates the cyst into individual sperm via actin-rich individualization complexes (ICs; Fabian and Brill, 2012). The ICs form around the nuclei at the proximal end of the cyst and progress evenly toward the distal end (Fig. 5 D). It is well established that defects in axoneme assembly, including loss of axonemal dynein motor proteins, perturb IC progression

(Fatima, 2011; Fingerhut et al., 2019; Wang et al., 2019). We found that RNAi-mediated knockdown of *rept* or *pont* does not affect IC assembly but does result in disorganized IC progression (Fig. 5, E-J), as is observed following knockdown of *kl-3*, *kl-5*, *kl-2*, or *Dhc98D* (Fig. S3; Fingerhut et al., 2019).

As previous studies have implicated Rept and Pont in male fertility and axonemal dynein motor assembly and the observed individualization defects are characteristic of axonemal defects, we analyzed Kl-3 protein levels following *rept* or *pont* RNAi. Western blotting using total testis extracts revealed that Kl-3 protein levels are drastically reduced following knockdown of *rept* or *pont* (Fig. 5 K). Taken together, our results demonstrate that Rept and Pont are required for mRNAs to congress in the kl-granule, which in turn is required for efficient translation. This defect in axonemal dynein expression is likely the cause of sterility in *rept* and *pont* RNAi testes, but it should be noted that due to the myriad of functions attributed to Rept and Pont (Mao and Houry, 2017; Robinson et al., 2013), it is possible that Rept and Pont play additional roles in the testis that are also important for fertility.

#### kl-granule formation and localization are required for cytoplasmic cilia maturation

Precise mRNA localization is a widely used mechanism to ensure that proteins are concentrated where they are needed (Medioni



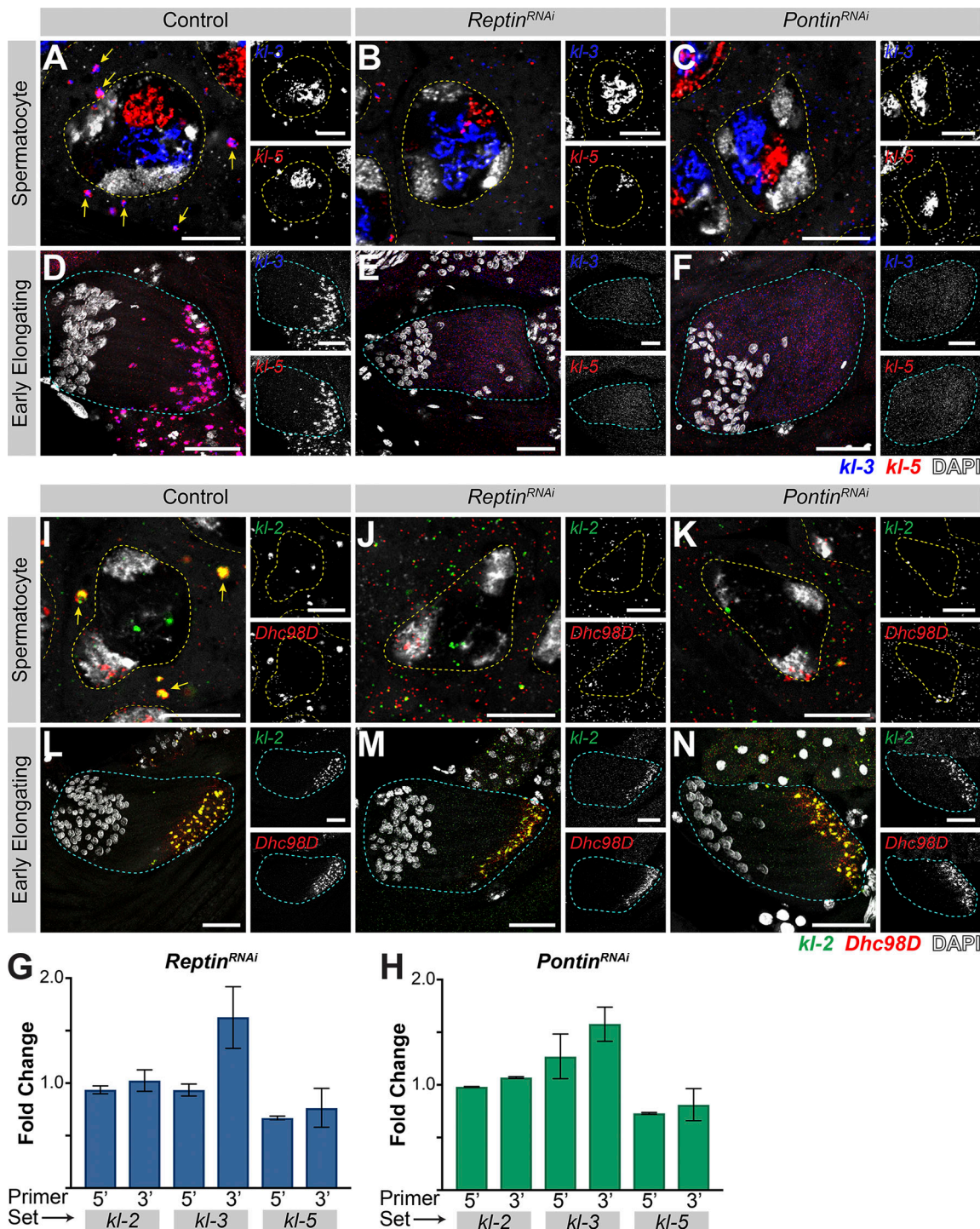


**Figure 4. Rept and Pont are required for kl-granule assembly.** (A–F) smFISH against *kl-3* and *kl-5* in control (A and D), *rept* RNAi (*bam-gal4>UAS-rept<sup>KK105732</sup>*; B and E), or *pont* RNAi (*bam-gal4>UAS-pont<sup>KK101103</sup>*; C and F) SCs (A–C, single z plane) and early elongating spermatids (D–F, z-projection). Shown are *kl-3* (blue), *kl-5* (red), DAPI (white), SC nuclei (yellow dashed lines), neighboring SC nuclei (narrow yellow dashed lines), SC kl-granules (yellow arrows), and a spermatid cyst (cyan dashed line). Scale bars: 10  $\mu$ m (A–C) or 25  $\mu$ m (D–F). (G and H) Quantitative RT-PCR in *rept* RNAi (*bam-gal4>UAS-rept<sup>KK105732</sup>*, G) or *pont* RNAi (*bam-gal4>UAS-pont<sup>KK101103</sup>*, H) for *kl-3*, *kl-5*, and *kl-2* using two primer sets per gene, as indicated (see Table S1). Data were normalized to GAPDH and sibling controls and represent at least two biological replicates, each reaction performed in technical triplicate. Error bars represent SD. (I–N) smFISH against *kl-2* and *Dhc98D* in control (I and L), *rept* RNAi (*bam-gal4>UAS-rept<sup>KK105732</sup>*, J and M), or *pont* RNAi (*bam-gal4>UAS-pont<sup>KK101103</sup>*; K and N) SCs (I–K, single z plane) and early elongating spermatids (L–N, z-projection). Shown are *kl-2* (green), *Dhc98D* (red), DAPI (white), SC nuclei (yellow dashed lines), neighboring SC nuclei (narrow yellow dashed lines), SC kl-granules (yellow arrows), and a spermatid cyst (cyan dashed line). Scale bars: 10  $\mu$ m (I–K) or 25  $\mu$ m (L–N).

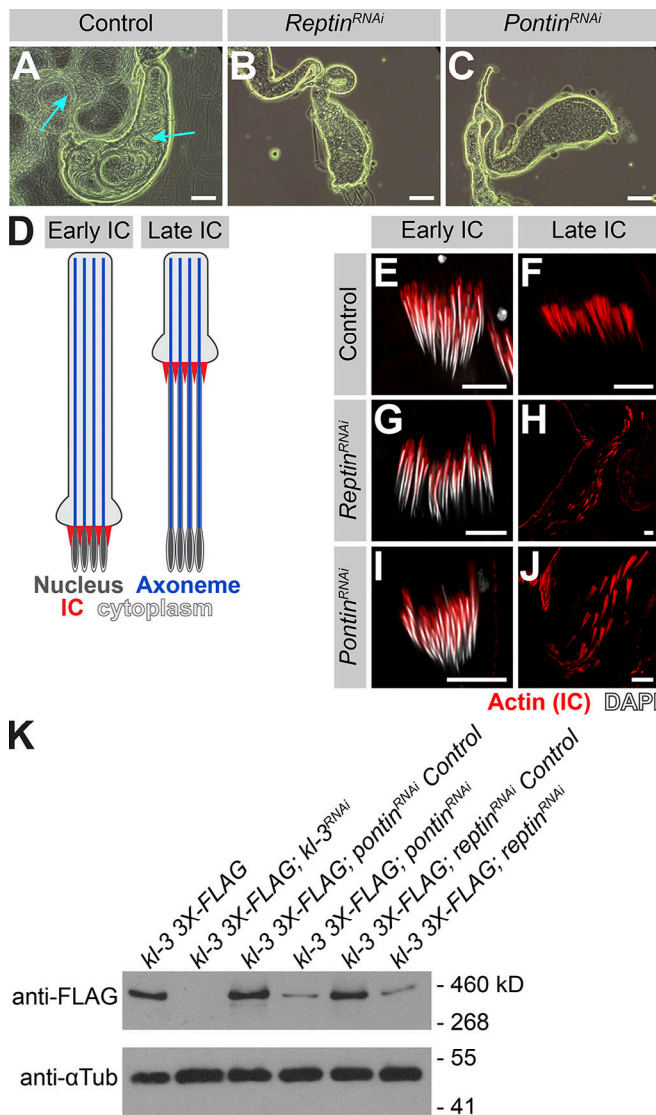


**Figure 5. kl-granule assembly is required for efficient Kl-3 translation and sperm motility.** (A–C) Phase-contrast images of seminal vesicles in control (A), *rept* RNAi (*bam-gal4>UAS-rept<sup>KK105732</sup>*; B), and *pont* RNAi (*bam-gal4>UAS-pont<sup>KK101103</sup>*; C). Cyan arrows point to mature sperm. Scale bars: 100  $\mu$ m. (D) Schematic of IC progression during individualization. Shown are the nucleus (dark gray), axoneme (blue), ICs (red), and cytoplasm (light gray). (E–J) Phalloidin staining of early and late ICs in the indicated genotypes. Shown are phalloidin (actin, red) and DAPI (white). Scale bars: 10  $\mu$ m. (K) Western blot for Kl-3-3X FLAG in the indicated genotypes.

et al., 2012). As described above, kl-granules localize to the distal end of elongating spermatids (Fig. 2), where bare axonemal microtubules are first exposed to the cytoplasm after being displaced from the ciliary cap as new microtubules are polymerized. We therefore postulated that the kl-granule may function in cytoplasmic cilia maturation. We first determined whether kl-granules localize within the ciliary cap or within the cytoplasmic compartment. By using Unc-GFP to mark the ring centriole, a structure at the base of the ciliary cap near the transition zone at the boundary between the cytoplasmic and compartmentalized regions (Baker et al., 2004; Phillips, 1970), we found that kl-granules are located within the cytoplasmic

compartment, immediately proximal to the ciliary cap (Fig. 6 A). Similarly, we found that FLAG-tagged Kl-3 protein (expressed from the endogenous locus; see Materials and methods) occupies the same region proximal to the ciliary cap as the kl-granules and that Kl-3 protein is restricted to the cytoplasmic compartment while the microtubules extend into the compartmentalized region (i.e., the ciliary cap; Fig. 6 B). These results indicate that while the axonemal microtubules are polymerized within the ciliary cap, axoneme maturation (the incorporation of axonemal dyneins and other axonemal proteins) may occur within the cytoplasmic compartment, as has been proposed (Avidor-Reiss and Leroux, 2015).

Detailed examination of Kl-3 protein within elongating spermatid cysts provided insights into where Kl-3 protein may be translated and incorporated into the growing axoneme (Fig. 6, C and D; and Fig. S4). Kl-3 protein is not present in SCs and becomes weakly detectable in round spermatids, but it does not robustly accumulate until elongating spermatids, where it becomes strongly enriched at the distal end, correlating with kl-granule localization (Figs. S4 and 2). At the distal end of the cyst, Kl-3 protein was predominantly observed in the cytoplasm while being excluded from the axonemal microtubules (Fig. 6 D; see the right panel for intensity plot showing mutually exclusive localization of microtubules and Kl-3). This suggests that Kl-3 protein at the distal end may represent the pool of newly translated Kl-3 before it is incorporated into the axoneme, which is also consistent with the presence of kl-granules at this location (Fig. S4). In contrast to the distal end, Kl-3 protein was observed to colocalize with axonemal microtubules at the proximal end (Fig. 6 D; see the right panel for intensity plot showing colocalization of microtubules and Kl-3), suggesting that Kl-3 protein has been successfully incorporated into the axoneme. These results suggest that Kl-3 protein may be translated at the distal end, where the kl-granules localize, and that the diffuse cytoplasmic Kl-3 protein may be the newly synthesized pool, which is subsequently incorporated into the axoneme.

Following RNAi-mediated knockdown of *rept* or *pont*, which prevents kl-granule formation (Fig. 4) and drastically reduces Kl-3 protein levels (Fig. 5 K), we still observed Kl-3 protein in the cytoplasm at the distal end (Fig. 6, F and H), although at a much reduced level. However, Kl-3 protein was never observed to colocalize with the axonemal microtubules at the proximal end upon *rept* or *pont* RNAi (Fig. 6, E and G), suggesting that Rept and Pont are required for incorporation of Kl-3 into the axoneme.

Consistent with this notion, transmission EM revealed that the ODAs and IDAs are largely absent from the axonemes following *rept* or *pont* RNAi (Fig. 6, I–K). Additional gross axonemal defects (e.g., broken axonemes) were present in the RNAi conditions (Fig. 6, L–N), suggesting additional impairments to axoneme assembly. These results suggest that mRNA localization via formation of kl-granules is required for axonemal dynein motor proteins to incorporate into the axoneme.

## Discussion

Cytoplasmic cilia have been found in organisms as diverse as *Plasmodium* and humans (Avidor-Reiss et al., 2017; Avidor-Reiss



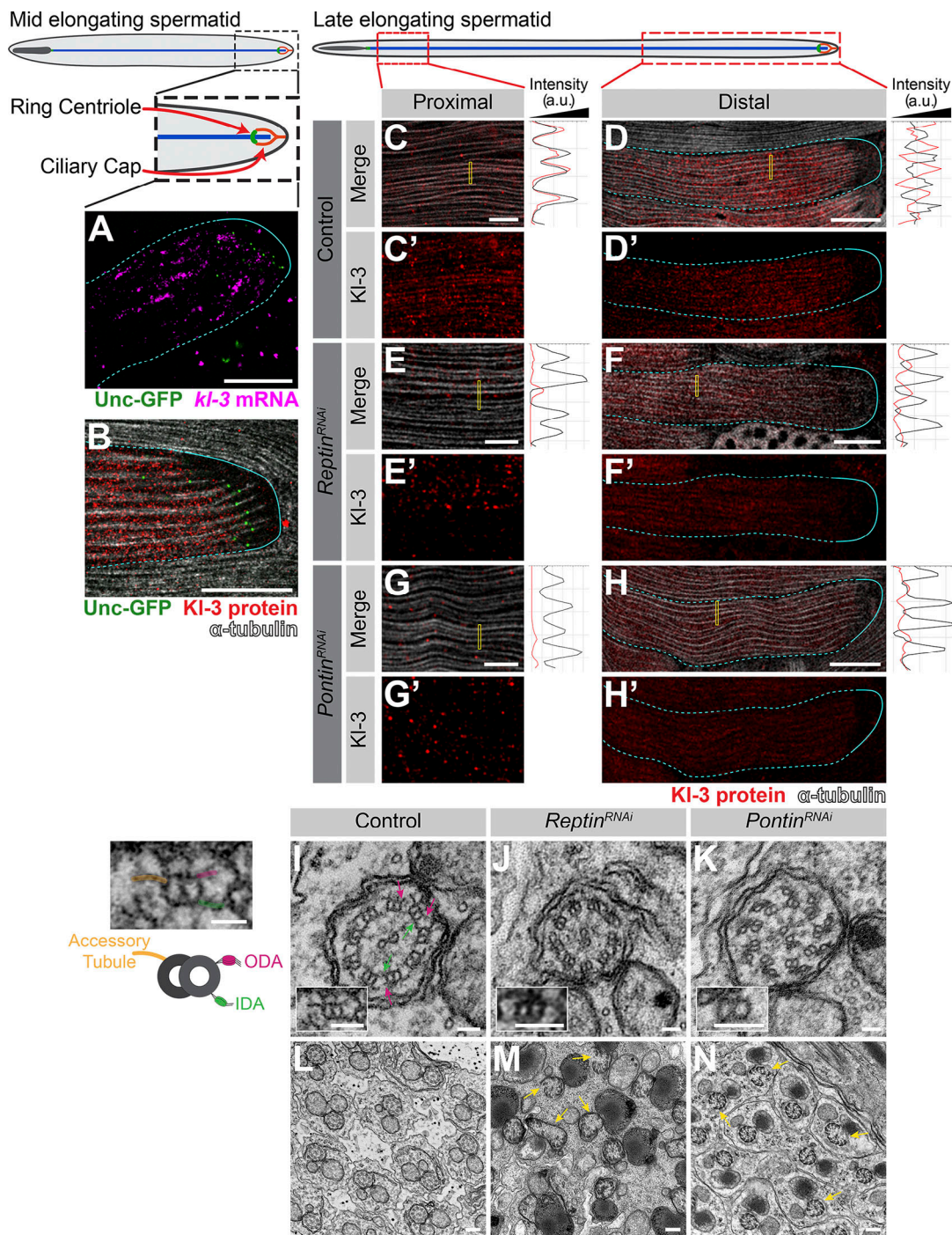


Figure 6. **kl-granule formation and localization are required for cytoplasmic cilia maturation.** (A) smFISH against *kl-3* in flies expressing Unc-GFP. Shown are *kl-3* (magenta), Unc-GFP (ring centriole, green), and a spermatid cyst (cyan, dashed line: cytoplasmic region; solid line: compartmentalized region). Scale bar: 20  $\mu$ m. (B) Kl-3-3X FLAG protein in flies expressing Unc-GFP. Shown are Kl-3 (red), Unc-GFP (ring centriole, green),  $\alpha$ -tubulin (white), and spermatid cyst (cyan, dashed line: cytoplasmic region, solid line: compartmentalized region). Scale bar: 20  $\mu$ m. (C–H) Kl-3-3X FLAG protein expression in control (C and D), *rept* RNAi (*bam-gal4>UAS-rept<sup>KK105732</sup>*; E and F), and *pont* RNAi (*bam-gal4>UAS-pont<sup>KK101103</sup>*; G and H) proximal (C, E, and G) and distal (D, F, and H) regions of late elongating spermatids. Shown are Kl-3 (red),  $\alpha$ -tubulin-GFP (white), and a spermatid cyst (cyan, dashed line: cytoplasmic region; solid line: compartmentalized region). Intensity plots are shown for the regions within the yellow rectangles. Scale bars: 5  $\mu$ m (C, E, and G) or 25  $\mu$ m (D, F, and H). (I–N) Transmission EM images of control (I and L), *rept* RNAi (*bam-gal4>UAS-rept<sup>KK105732</sup>*; J and M), and *pont* RNAi (*bam-gal4>UAS-pont<sup>KK101103</sup>*; K and N) axonemes. Magenta arrows, ODA; green arrows, IDA; yellow arrows, broken axonemes. The control single doublet enlarged image is duplicated to the left of the figure and colored to match the diagram. Scale bars: 50 nm (I–K), 200 nm (L–N), or 25 nm (diagram left of I).

and Leroux, 2015; Dawson and House, 2010; Fawcett et al., 1970; Sinden et al., 1976; Tates, 1971; Tokuyasu, 1975). While it has been proposed that axoneme maturation proceeds through the direct incorporation of axonemal proteins from the cytoplasm, this model remained untested (Avidor-Reiss and Leroux, 2015). Our study provides the first insights into the mechanism of cytoplasmic cilia formation. Our results show that localization of axonemal dynein mRNAs facilitates the maturation of cytoplasmic cilia by concentrating axonemal dynein proteins, likely through localized translation, allowing for the efficient incorporation of axonemal dynein proteins into bare axonemal microtubules directly from the cytoplasm.

### Mechanism for cytoplasmic cilia maturation

It has been proposed that cytoplasmic cilia assemble in two steps (Avidor-Reiss and Leroux, 2015): first, microtubules are polymerized within a small compartmentalized region of the cilia; then, as the bare microtubules are displaced from this region, axonemal proteins are incorporated directly from the cytoplasm during the maturation step. Previous studies that have shown that IFT, the process used by traditional compartmentalized cilia to ferry axonemal proteins into the ciliary compartment, is dispensable for *Drosophila* spermiogenesis, and that the genomes of some other organisms known to form cytoplasmic cilia (e.g., *Plasmodium*) do not encode IFT and/or transition zone proteins (Avidor-Reiss and Leroux, 2015; Avidor-Reiss et al., 2004; Breslow et al., 2013; Briggs et al., 2004; Han et al., 2003; Hoeng et al., 2008; Kee et al., 2012; Lin et al., 2013; Sarpal et al., 2003). These studies led to the notion that maturation of cytoplasmic cilia ought to happen in the cytoplasm, although direct evidence has been lacking.

Our study, which identified a novel RNP granule, the kl-granule, composed of axonemal dynein heavy chain mRNAs and the proteins Rept and Pont, provides the first molecular insights into cytoplasmic cilia maturation. Our results show that axonemal dynein heavy chain mRNAs (*kl-3*, *kl-5*, *kl-2*, and *Dhc98D*) congress into kl-granules in SCs. We further show that Rept and Pont are required for kl-granule assembly and the robust translation of axonemal dynein mRNAs. We demonstrate that the polarized localization of kl-granule mRNAs and their protein products within the cytoplasmic compartment allows for the incorporation of axonemal dyneins into the axoneme, facilitating the maturation step in cytoplasmic cilia assembly (Fig. 7). Our results refine the proposed two-step model for cytoplasmic cilia assembly by demonstrating that concentrating axonemal proteins within distal regions of the cytoplasm is critical for maturation. Our data suggest that kl-granule mRNAs are locally translated at the distal end as *kl-3* mRNA and Kl-3 protein are both polarized at this end (Figs. S4 and 6), although we cannot exclude other alternative possibilities. Thus, axoneme maturation proceeds in a stepwise fashion, allowing for the efficient assembly of this very long cilia. This model implies that the proximal region of the axoneme is more mature than the distal region, as axonemal proteins are still cytoplasmic at the distal end while they have incorporated at the proximal end, a notion that is supported by previous studies that looked at axoneme ultrastructure and

tubulin dynamics within the axoneme (Noguchi et al., 2011; Sinden et al., 2010; Tokuyasu, 1975).

### Function of Rept and Pont in dynein assembly

A wide range of functions have been assigned to Rept- and Pont-containing complexes, including roles in chromatin remodeling, transcription regulation, DNA repair, and ribosome assembly (Mao and Houry, 2017). They can act alone, together, or as part of larger complexes (Huen et al., 2010; Kakiyama and Saeki, 2014). Among these, previous studies have proposed that Rept and Pont are dynein arm preassembly factors, chaperones that take individual dynein motor subunits (i.e., the heavy, intermediate, and light chain proteins) and stabilize and assemble them into a motor unit in the cytoplasm that is then ferried into the cilia for incorporation (Desai et al., 2018; Fabczak and Osinka, 2019; Fowkes and Mitchell, 1998). These assembly factors include R2TP and R2TP-like complexes (which include Rept [RUVBL2] and Pont [RUVBL1]) in association with dynein axonemal assembly factors (Fabczak and Osinka, 2019). Our data suggest that Rept and Pont are involved in RNP complex assembly. While previous studies have demonstrated that Rept, Pont, R2TP, and dynein axonemal assembly factors are needed for axonemal dynein incorporation (Huizar et al., 2018; Li et al., 2017; Liu et al., 2019; Yamaguchi et al., 2018; Zhao et al., 2013; Zur Lage et al., 2018), our study is the first to demonstrate the importance of axonemal dynein mRNAs with these complexes, showing that Rept and Pont are required for axonemal dynein mRNAs to localize to kl-granules. We cannot however exclude the possibility that Rept and Pont may also be playing more traditional roles in protein stability (Kl-3 protein may be translated in the *rept* and *pont* RNAi conditions but degraded due to lack of chaperone activity) or complex assembly (similarly, Kl-3 protein may be translated but degraded if it cannot complex with dynein intermediate and light chains). Interestingly, a recent study reported the presence of RNA in dynein assembly complexes in *Xenopus* multiciliated cells (Drew et al., 2020 Preprint), and while the identity of these RNAs is unknown, it is intriguing to postulate that similarities may exist between kl-granules and these previously identified dynein assembly particles. However, important differences exist as well. First, while *kl-3* mRNA is present in kl-granules, no puncta are observed for Kl-3 protein (Figs. 6 and S4), indicating that Kl-3 protein does not concentrate within kl-granules (or another granule) as dyneins do in the dynein preassembly complexes reported in other systems (Dafinger et al., 2018; Huizar et al., 2018). Additionally, dynein preassembly complexes were found to contain proteins (e.g., Wdr78 [Huizar et al., 2018]), where the *Drosophila* homologue (*Dic61B*) mRNAs are not constituents of the kl-granules (Fig. S5; see below). Therefore, the kl-granule may be a novel adaptation of a Rept- and Pont-containing dynein arm assembly complex specifically found in cytoplasmic cilia and is distinct from its role as a dynein preassembly factor in other systems.

It is likely that additional protein components of the kl-granule remain to be discovered. Structural analyses in previous studies have identified mechanisms by which other proteins interact with Rept and Pont (Rivera-Calzada et al., 2017); however, Rept and Pont do not have any RNA-binding domains (Mao

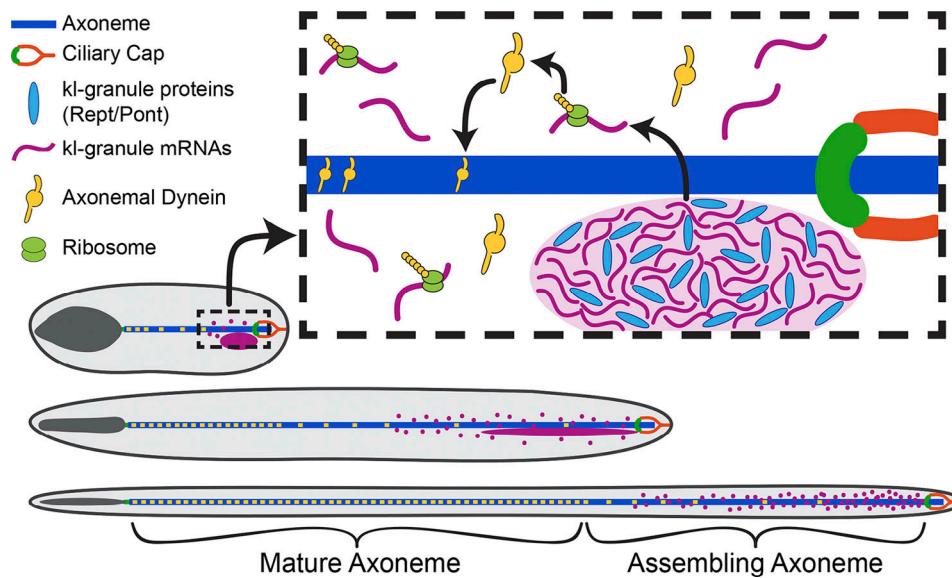


Figure 7. **Model for cytoplasmic cilia maturation.** The kl-granule (light purple) localizes immediately proximal to the ciliary cap (orange) and transition zone (green) within the cytoplasmic compartment. Constituent mRNAs (purple) are likely locally translated (ribosomes, lime green), and their proteins (axonemal dyneins, yellow) are incorporated into the axoneme (blue) as the microtubules are displaced from the ciliary cap. In this way, cytoplasmic cilia maturation is progressive, with axonemal proteins being added to the bare microtubules as elongation proceeds.

and Houry, 2017). Therefore, it is likely that additional proteins, not Rept and Pont themselves, physically interact with constituent mRNAs for kl-granule formation. Our data also support the existence of additional proteins governing kl-granule dynamics. For example, as spermatids elongate, the ODA and IDA mRNAs separate slightly from each other while remaining polarized at the distal end (Fig. 2). Moreover, in the absence of Rept and Pont, the IDA mRNAs are still able to congress at the distal end of the elongating spermatid cyst, after failing to form kl-granules in SCs. In contrast, localization of the ODA mRNAs entirely depends on Rept and Pont, as ODA mRNAs remain diffuse throughout spermatogenesis following *rept* or *pont* RNAi. Finally, Pont more strongly colocalizes with the ODA mRNAs within the kl-granule (Fig. 3 F), which altogether suggests that there are additional proteins that can sort and specify the fate of these kl-granule mRNAs both alongside or in the absence of Rept and Pont. The identity of these additional proteins is the subject of further study. Alternatively, there could be a differential requirement for Rept and Pont and/or their associated proteins between ODA and IDA mRNAs and over developmental time. Determining the involvement of the other dynein arm pre-assembly factors is of particular interest, especially considering the existence of multiple dynein arm assembly complexes that have been shown to differentially regulate IDA and ODA assembly (Fabczak and Osinka, 2019; Yamaguchi et al., 2018). It is also appealing to posit the existence of testis-specific factors that may help to distinguish the role of Rept and Pont in cytoplasmic cilia formation from their role in the assembly of other cellular bodies.

#### Purpose of mRNA localization to kl-granules

Interestingly, we found that not all mRNAs for axonemal/spermiogenesis proteins localize to kl-granules (Fig. S5). mRNAs for

other axonemal proteins (the dynein intermediate chain *Dic61B*, the dynein heavy chain CG3339, and the ODA docking complex component CG17083; Zur Lage et al., 2019), as well as mRNAs for other Y-linked transcripts (*CCY* and *PPR-Y*; Carvalho et al., 2001) and a nonaxonemal spermatid protein (*fzo*; Hales and Fuller, 1997), did not localize to kl-granules. Instead they remain evenly distributed throughout the cytoplasm, despite also being important for sperm maturation (Fig. S5). Additionally, we previously reported that mRNAs for the Y-linked gene *ORY* also gather in cytoplasmic RNA granules in late SCs (Fingerhut et al., 2019); however, these RNA granules are distinct from the kl-granule (Fig. S5, F and G).

In particular, it is intriguing that *Dic61B* mRNA, an IDA intermediate chain that needs to bind to the IDA heavy chains Kl-2 and Dhc98D, is located differently (diffusely) within the spermatid cyst. Dynein preassembly is believed to be important for dynein protein stability and a prerequisite for axonemal incorporation (Fabczak and Osinka, 2019; Fowkes and Mitchell, 1998). An intriguing possibility is that temporal/spatial regulation of dynein mRNAs plays a role in helping the ordered assembly of dynein complexes. It will be of future interest to determine when and where during spermiogenesis dynein complexes are formed in the cytoplasmic cilia as well as what factors are necessary for their formation. A comprehensive understanding of kl-granule mRNAs and proteins would allow for further study into this temporal/spatial regulatory mechanism and a more thorough understanding of how kl-granules function in the maturation of cytoplasmic cilia.

In summary, our study provides the first insights into the mechanism of cytoplasmic cilia maturation: mRNAs for axonemal dynein motor proteins are localized at the distal end of the axoneme within the cytoplasmic compartment, which allows for efficient maturation of cytoplasmic cilia.



## Materials and methods

### Fly husbandry

All fly stocks were raised on standard Bloomington medium at 25°C, and young flies (1- to 5-d-old adults) were used for all experiments. Flies used for wild-type experiments were the standard laboratory wild-type strain *yw* ( $y^1w^1$ ). The following fly stocks were used: *bam-GAL4:VP16* (Bloomington *Drosophila* Stock Center [BDSC]: 80579), *UAS-kl-3<sup>TRIP.HMC03546</sup>* (BDSC: 53317), *UAS-kl-5<sup>TRIP.HMC03747</sup>* (BDSC:55609), *UAS-Dhc98D<sup>TRIP.HMC06494</sup>* (BDSC: 77181), and *C(1)RM/C(1;Y)6, y<sup>1</sup>w<sup>1</sup>/0* (BDSC: 9460) were obtained from the BDSC. *UAS-kl-2<sup>GC8807</sup>* (Vienna *Drosophila* Resource Center [VDR]: v19181), *UAS-rept<sup>KKI05732</sup>* (VDR: v103483), and *UAS-pont<sup>KKI01103</sup>* (VDR: v105408) were obtained from the VDR. *unc-GFP* (GFP-tagged *unc* expressed by the endogenous promoter) and *Ub- $\alpha$ -tubulin84B-GFP* were a gift from Cayetano Gonzalez (IRB Barcelona, Barcelona, Spain; Baker et al., 2004; Rebollo et al., 2004), and *bam-gal4* was a gift from Dennis McKearin (Howard Hughes Medical Institute, Chevy Chase, MD; Chen and McKearin, 2003). The *kl-3-FLAG* strain was constructed using CRISPR-mediated knock-in of a 3X-FLAG tag at the C-terminus of *kl-3* as previously described (Fingerhut et al., 2019).

### smFISH

All solutions used for RNA FISH were RNase-free. Testes from 2- to 3-d-old flies were dissected in 1X PBS and fixed in 4% formaldehyde in 1X PBS for 30 min. Then testes were washed briefly in 1X PBS and permeabilized in 70% ethanol overnight at 4°C. Testes were briefly rinsed with wash buffer (2X saline-sodium citrate, 10% formamide) and then hybridized overnight at 37°C in hybridization buffer containing 2X saline-sodium citrate, 10% dextran sulfate (Sigma-Aldrich; D8906), 1 mg/ml *Escherichia coli* tRNA (Sigma-Aldrich; R8759), 2 mM Vanadyl Ribonucleoside complex (NEB; S142), 0.5% BSA (Ambion; AM2618), and 10% formamide. Following hybridization, samples were washed three times in wash buffer for 20 min each at 37°C and mounted in VECTASHIELD with DAPI (Vector Labs). Images were acquired using an upright Leica TCS SP8 confocal microscope with a 63 $\times$  oil immersion objective lens (NA 1.4) and processed using Adobe Photoshop and ImageJ software.

Fluorescently labeled probes were added to the hybridization buffer to a final concentration of 100 nM. Probes against *kl-3*, *kl-5*, *kl-2*, *Dhc98D*, *CG3339*, *Dic61B*, *CG17083*, *CCY*, *PPR-Y*, *ORY*, and *fzo* mRNAs were designed using the Stellaris RNA FISH Probe Designer (Biosearch Technologies; available online at [www.biosearchtech.com/stellarisdesigner](http://www.biosearchtech.com/stellarisdesigner)). Each set of custom Stellaris RNA FISH probes was labeled with Quasar 670, Quasar 570, or Fluorescein (Table S1).

For strains expressing GFP (e.g., *unc-GFP* or *Ub- $\alpha$ -tubulin84B-GFP*), the overnight permeabilization in 70% ethanol was omitted.

### Immunofluorescence staining

Testes were dissected in 1X PBS, transferred to 4% formaldehyde in 1X PBS, and fixed for 30 min. Testes were then washed in 1X PBST (PBS containing 0.1% Triton X-100) for at least 60 min followed by incubation with primary antibodies diluted in 1X

PBST with 3% BSA at 4°C overnight. Samples were washed for at least 1 h in 1X PBST, incubated with secondary antibody in 1X PBST with 3% BSA at 4°C overnight, washed as above, and mounted in VECTASHIELD with DAPI (Vector Labs). Images were acquired using an upright Leica TCS SP8 confocal microscope with a 63 $\times$  oil immersion objective lens (NA 1.4) and processed using Adobe Photoshop and ImageJ software.

The following primary antibodies were used: anti- $\alpha$ -tubulin (1:100, mouse; Sigma-Aldrich; T6199), anti-FLAG (1:500, rabbit; Invitrogen; PA1-984B), anti-Rept (1:200, rabbit, gift of Andrew Saurin, Institut de Biologie du Développement de Marseille, Marseille, France [Diop et al., 2008]), anti-Pont (1:200; guinea pig, this study), Phalloidin-Alexa Fluor 546 or 488 (1:200; Thermo Fisher Scientific; A22283 or A12379). The Pont antibody was generated by injecting a peptide (CKVNGRNQISKDDIEDVH, targeting 18 aa from the C-terminal end of Pont) in guinea pigs (Covance). Alexa Fluor-conjugated secondary antibodies (Life Technologies) were used at a dilution of 1:200.

A modified version of Stefanini's fixative (4% formaldehyde, 0.18% wt/vol picric acid [Ricca Chemical 5860], 0.3 M Pipes, pH 7.5 [Alfa Aesar; J63617], and 0.05% Tween-20) was used in order to detect Kl-3 (Müller, 2008). No signal was detectable using traditional formaldehyde fixation.

### Immunofluorescence staining with smFISH

To combine immunofluorescent staining with smFISH, testes from 2- to 3 d-old-flies were dissected in 1X PBS and fixed in 4% formaldehyde in 1X PBS for 30 min. Then testes were washed briefly in PBS and permeabilized in 70% ethanol overnight at 4°C (unless from a strain expressing GFP, in which case this step was omitted). Testes were then washed with 1X PBS and blocked for 30 min at 37°C in blocking buffer (1X PBS, 0.05% BSA, 50  $\mu$ g/ml *E. coli* tRNA, 10 mM Vanadyl Ribonucleoside complex, and 0.2% Tween-20). Primary antibodies were diluted in blocking buffer and incubated at 4°C overnight. The testes were washed with 1X PBS containing 0.2% Tween-20, reblocked for 5 min at 37°C in blocking buffer, and incubated 4°C overnight in blocking buffer containing secondary antibodies. Then, testes were washed with 1X PBS containing 0.2% Tween-20 and refixed for 10 min before continuing the smFISH, starting from the brief rinse with wash buffer.

### Quantitative RT-PCR

Total RNA from testes (50 pairs/sample) was extracted using TRIzol (Invitrogen) according to the manufacturer's instructions. 1  $\mu$ g total RNA was reverse transcribed using SuperScript III Reverse transcription (Invitrogen) followed by qPCR using Power SYBR Green reagent (Applied Biosystems) on a QuantStudio 6 Real-Time PCR system (Applied Biosystems). Primers for quantitative PCR were designed to amplify only mRNA. The genes analyzed by qPCR are all predicted to contain megabase sized introns, and primers were designed to span these large introns such that a product would be detected only if the intron had been spliced out (Fingerhut et al., 2019). Two primer sets were used for each gene, one near the 5' end and another closer to the 3' end. Relative expression levels were normalized to GAPDH and cross-sibling controls. All reactions

were done in technical triplicates with at least two biological replicates. Graphical representation is inclusive of all replicates. Primers used are listed in Table S1.

### Western blot

Testes (40 pairs/sample) were dissected in Schneider's media at room temperature within 30 min, the media was removed, and the samples were frozen at  $-80^{\circ}\text{C}$  until use. After thawing, testes were then lysed in 200  $\mu\text{l}$  of 2X Laemmli Sample Buffer +  $\beta\text{ME}$  (Bio-Rad; 161-0737). For Kl-3, samples were separated on a NuPAGE Tris-Acetate gel (Invitrogen; 3–8%, 1.5 mm), and for Rept and Pont, samples were separated on a Novex Tris-Glycine gel (Invitrogen; 10%, 1 mm) with the appropriate running buffer in a Xcell SureLock mini-cell electrophoresis system (Invitrogen). For Kl-3, proteins were transferred using the XCell II blot module (Invitrogen) onto a polyvinylidene fluoride membrane (Immobilon-P, Millipore) using NuPAGE transfer buffer (Invitrogen) without added methanol. For Rept and Pont, transfer buffer contained 20% methanol. Membranes were blocked in 1X TBST (0.1% Tween-20) containing 5% nonfat milk, followed by incubation with primary antibodies diluted in 1X TBST containing 5% nonfat milk. Membranes were washed with 1X TBST, followed by incubation with secondary antibodies diluted in 1X TBST containing 5% nonfat milk. After washing with 1X TBST, detection was performed using the Pierce ECL Western Blotting Substrate enhanced chemiluminescence system (Thermo Fisher Scientific). Primary antibodies used were anti- $\alpha$ -tubulin (1:2,000, mouse; Sigma-Aldrich; T6199), anti-FLAG (1:2,500, mouse; Sigma-Aldrich; F1804), anti-Rept (1:2,000, rabbit; gift of Andrew Saurin), anti-Pont (1:2,000, guinea pig; this study), and anti-Vasa (1:3,000, rabbit; Santa Cruz Biotechnology; D-260). The secondary antibodies were HRP-conjugated goat anti-mouse IgG, anti-rabbit IgG, or anti-guinea pig IgG (1:10,000; Abcam).

### Phase contrast microscopy

Seminal vesicles were dissected in 1X PBS and transferred to slides for live observation by phase contrast on a Leica DM5000B microscope with a 40 $\times$  objective (NA 0.75) and imaged with a QImaging Retiga 2000R Fast 1394 Mono Cooled camera. Images were adjusted in Adobe Photoshop.

### Transmission EM

Testes were fixed for 1 h or overnight (at  $4^{\circ}\text{C}$ ) with 2.5% glutaraldehyde in 0.1M Sorensen's buffer, pH 7.4. Samples were rinsed twice for 5 min each with 0.1 M Sorensen's buffer and postfixed for 1 h in 1% osmium tetroxide in 0.1 M Sorensen's buffer. Next, testes were rinsed twice in double distilled water for 5 min each and en bloc stained with 2% uranyl acetate in double distilled water for 1 h. The samples were then dehydrated in increasing concentrations of ethanol, rinsed with acetone, and embedded in epon epoxy resin. Thin sections were mounted on Formvar/carbon-coated slotted grids and poststained with uranyl acetate and lead citrate. Samples were examined on a JEOL1400 transmission electron microscope and images captured using a sCMOS XR401 custom engineered optic camera by AMT (Advanced Microscopy Techniques).

### Fingerhut and Yamashita

mRNA localization in sperm cilia maturation

### Online supplemental material

Fig. S1 shows efficiency of RNAi knockdown of *kl-3*, *kl-5*, *kl-2*, and *Dhc98D* by smFISH and lack of dependence upon a one of those transcripts for kl-granule formation (related to Fig. 1). Fig. S2 shows that RNAi of *rept* or *pont* results in efficient knockdown of both products (related to Fig. 4). Fig. S3 shows the sterility phenotype of *kl-3*, *kl-5*, *kl-2*, and *Dhc98D* RNAi flies (related to Fig. 5). Fig. S4 shows Kl-3 protein distribution and stage-matched *kl-3* mRNA (related to Fig. 6). Fig. S5 shows smFISH for other axonemal, Y-linked, and spermatid-essential transcripts (related to Discussion).

### Acknowledgments

We thank Drs. Dennis McKearin, Cayetano Gonzalez, and Andrew Saurin, the BDSC, and the VDRG for reagents. We thank Sasha Meshinchi and the University of Michigan Microscopy Core for help with EM experiments. We thank the Yamashita laboratory and Drs. Sue Hammoud and Joshua Bembenek for discussion and comments on the manuscript, Drs. Tomer Avidor-Reiss and Tony Mahowald for helpful suggestions, and Dr. Jiandie Lin (University of Michigan, Ann Arbor, MI) for sharing equipment.

This work was supported by the Howard Hughes Medical Institute (Y.M. Yamashita) and National Institutes of Health cellular and molecular biology training grant T32-GM007315 (J.M. Fingerhut).

The authors declare no competing financial interests.

Author contributions: J.M. Fingerhut conceived the project and conducted experiments. J.M. Fingerhut and Y.M. Yamashita designed experiments, analyzed the data, and wrote the manuscript.

Submitted: 13 March 2020

Revised: 10 June 2020

Accepted: 15 June 2020

### References

- Anderson, P., and N. Kedersha. 2009. RNA granules: post-transcriptional and epigenetic modulators of gene expression. *Nat. Rev. Mol. Cell Biol.* 10: 430–436. <https://doi.org/10.1038/nrm2694>
- Avidor-Reiss, T., and M.R. Leroux. 2015. Shared and Distinct Mechanisms of Compartmentalized and Cytosolic Ciliogenesis. *Curr. Biol.* 25:R1143–R1150. <https://doi.org/10.1016/j.cub.2015.11.001>
- Avidor-Reiss, T., A.M. Maer, E. Koundakjian, A. Polyanovsky, T. Keil, S. Subramaniam, and C.S. Zuker. 2004. Decoding cilia function: defining specialized genes required for compartmentalized cilia biogenesis. *Cell.* 117:527–539. [https://doi.org/10.1016/S0092-8674\(04\)00412-X](https://doi.org/10.1016/S0092-8674(04)00412-X)
- Avidor-Reiss, T., A. Ha, and M.L. Basiri. 2017. Transition Zone Migration: A Mechanism for Cytoplasmic Ciliogenesis and Postaxonemal Centriole Elongation. *Cold Spring Harb. Perspect. Biol.* 9:a028142. <https://doi.org/10.1101/cshperspect.a028142>
- Baker, J.D., S. Adhikarakunnathu, and M.J. Kernan. 2004. Mechanosensory-defective, male-sterile unc mutants identify a novel basal body protein required for ciliogenesis in Drosophila. *Development.* 131:3411–3422. <https://doi.org/10.1242/dev.01229>
- Barckmann, B., X. Chen, S. Kaiser, S. Jayaramaiah-Raja, C. Rathke, C. Dottermusch-Heidel, M.T. Fuller, and R. Renkawitz-Pohl. 2013. Three levels of regulation lead to protamine and Mst77F expression in Drosophila. *Dev. Biol.* 377:33–45. <https://doi.org/10.1016/j.ydbio.2013.02.018>

- Basiri, M.L., A. Ha, A. Chadha, N.M. Clark, A. Polyansky, B. Cook, and T. Avidor-Reiss. 2014. A migrating ciliary gate compartmentalizes the site of axoneme assembly in *Drosophila* spermatids. *Curr. Biol.* 24: 2622–2631. <https://doi.org/10.1016/j.cub.2014.09.047>
- Bley, N., M. Lederer, B. Pfalz, C. Reinke, T. Fuchs, M. Gläß, B. Möller, and S. Hüttelmaier. 2015. Stress granules are dispensable for mRNA stabilization during cellular stress. *Nucleic Acids Res.* 43. e26. <https://doi.org/10.1093/nar/gku1275>
- Boisvert, F.M., S. van Koningsbruggen, J. Navascués, and A.I. Lamond. 2007. The multifunctional nucleolus. *Nat. Rev. Mol. Cell Biol.* 8:574–585. <https://doi.org/10.1038/nrm2184>
- Breslow, D.K., E.F. Koslover, F. Seydel, A.J. Spakowitz, and M.V. Nachury. 2013. An *in vitro* assay for entry into cilia reveals unique properties of the soluble diffusion barrier. *J. Cell Biol.* 203:129–147. <https://doi.org/10.1083/jcb.201212024>
- Briggs, L.J., J.A. Davidge, B. Wickstead, M.L. Ginger, and K. Gull. 2004. More than one way to build a flagellum: comparative genomics of parasitic protozoa. *Curr. Biol.* 14:R611–R612. <https://doi.org/10.1016/j.cub.2004.07.041>
- Buchan, J.R.. 2014. mRNP granules. Assembly, function, and connections with disease. *RNA Biol.* 11:1019–1030. <https://doi.org/10.4161/15476286.2014.972208>
- Carvalho, A.B., B.P. Lazzaro, and A.G. Clark. 2000. Y chromosomal fertility factors kl-2 and kl-3 of *Drosophila melanogaster* encode dynein heavy chain polypeptides. *Proc. Natl. Acad. Sci. USA.* 97:13239–13244. <https://doi.org/10.1073/pnas.230438397>
- Carvalho, A.B., B.A. Dobo, M.D. Vibriantovski, and A.G. Clark. 2001. Identification of five new genes on the Y chromosome of *Drosophila melanogaster*. *Proc. Natl. Acad. Sci. USA.* 98:13225–13230. <https://doi.org/10.1073/pnas.231484998>
- Caudron, F., and Y. Barral. 2009. Septins and the lateral compartmentalization of eukaryotic membranes. *Dev. Cell.* 16:493–506. <https://doi.org/10.1016/j.devcel.2009.04.003>
- Chen, D., and D.M. McKeearin. 2003. A discrete transcriptional silencer in the bam gene determines asymmetric division of the *Drosophila* germline stem cell. *Development.* 130:1159–1170. <https://doi.org/10.1242/dev.00325>
- Dafinger, C., M.M. Rinschen, L. Borgeal, C. Ehrenberg, S.G. Basten, M. Franke, M. Höhne, M. Rauh, H. Göbel, W. Bloch, et al. 2018. Targeted deletion of the AAA-ATPase Ruvb1 in mice disrupts ciliary integrity and causes renal disease and hydrocephalus. *Exp. Mol. Med.* 50:1–17. <https://doi.org/10.1038/s12276-018-0108-z>
- Dawson, S.C., and S.A. House. 2010. Life with eight flagella: flagellar assembly and division in *Giardia*. *Curr. Opin. Microbiol.* 13:480–490. <https://doi.org/10.1016/j.mib.2010.05.014>
- Desai, P.B., A.B. Dean, and D.R. Mitchell. 2018. Cytoplasmic preassembly and trafficking of axonemal dyneins. *Dyneins.* 1:140–161.
- Diop, S.B., K. Bertaux, D. Vasanthi, A. Sarkeshik, B. Goirand, D. Aragnol, N.S. Tolwinski, M.D. Cole, J. Pradel, J.R. Yates, III, et al. 2008. Reptin and Pontin function antagonistically with PcG and TrxG complexes to mediate Hox gene control. *EMBO Rep.* 9:260–266. <https://doi.org/10.1038/embor.2008.8>
- Drew, K., C. Lee, R.M. Cox, V. Dang, C.C. Devitt, O. Papoulas, R.L. Huizar, E.M. Marcotte, and J.B. Wallingford. 2020. A systematic, label-free method for identifying RNA-associated proteins *in vivo* provides insights into vertebrate ciliary beating. *bioRxiv*. doi: 10.1101/2020.02.26.966754 Preprint posted March 2, 2020.
- Fabczak, H., and A. Osinka. 2019. Role of the Novel Hsp90 Co-Chaperones in Dynein Arms' Preassembly. *Int. J. Mol. Sci.* 20:6174. <https://doi.org/10.3390/ijms20246174>
- Fabian, L., and J.A. Brill. 2012. *Drosophila* spermiogenesis: Big things come from little packages. *Spermatogenesis.* 2:197–212. <https://doi.org/10.4161/spmg.21798>
- Fatima, R.. 2011. *Drosophila* Dynein intermediate chain gene, Dic61B, is required for spermatogenesis. *PLoS One.* 6. e27822. <https://doi.org/10.1371/journal.pone.0027822>
- Fawcett, D.W., E.M. Eddy, and D.M. Phillips. 1970. Observations on the fine structure and relationships of the chromatoid body in mammalian spermatogenesis. *Biol. Reprod.* 2:129–153. <https://doi.org/10.1095/biolreprod2.1.129>
- Fingerhut, J.M., J.V. Moran, and Y.M. Yamashita. 2019. Satellite DNA-containing gigantic introns in a unique gene expression program during *Drosophila* spermatogenesis. *PLoS Genet.* 15. e1008028. <https://doi.org/10.1371/journal.pgen.1008028>
- Fowkes, M.E., and D.R. Mitchell. 1998. The role of preassembled cytoplasmic complexes in assembly of flagellar dynein subunits. *Mol. Biol. Cell.* 9: 2337–2347. <https://doi.org/10.1091/mbc.9.9.2337>
- Fuller, M.T.. 1993. Spermatogenesis. In *The Development of Drosophila melanogaster*. Vol. 1. M. Bate, and A.M. Arias, editors. Cold Spring Harbor Laboratory Press, New York. pp. 71–148.
- Goldstein, L.S., R.W. Hardy, and D.L. Lindsley. 1982. Structural genes on the Y chromosome of *Drosophila melanogaster*. *Proc. Natl. Acad. Sci. USA.* 79: 7405–7409. <https://doi.org/10.1073/pnas.79.23.7405>
- Gorynia, S., T.M. Bandejas, F.G. Pinho, C.E. McVey, C. Vonnrhein, A. Round, D.I. Svergun, P. Donner, P.M. Matias, and M.A. Carrondo. 2011. Structural and functional insights into a dodecameric molecular machine - the RuvBL1/RuvBL2 complex. *J. Struct. Biol.* 176:279–291. <https://doi.org/10.1016/j.jsb.2011.09.001>
- Gottardo, M., G. Callaini, and M.G. Riparbelli. 2013. The cilium-like region of the *Drosophila* spermatocyte: an emerging flagellum? *J. Cell Sci.* 126: 5441–5452. <https://doi.org/10.1242/jcs.136523>
- Hales, K.G., and M.T. Fuller. 1997. Developmentally regulated mitochondrial fusion mediated by a conserved, novel, predicted GTPase. *Cell.* 90: 121–129. [https://doi.org/10.1016/S0092-8674\(00\)80319-0](https://doi.org/10.1016/S0092-8674(00)80319-0)
- Han, Y.G., B.H. Kwok, and M.J. Kernan. 2003. Intraflagellar transport is required in *Drosophila* to differentiate sensory cilia but not sperm. *Curr. Biol.* 13:1679–1686. <https://doi.org/10.1016/j.cub.2003.08.034>
- Hardy, R.W., K.T. Tokuyasu, and D.L. Lindsley. 1981. Analysis of spermatogenesis in *Drosophila melanogaster* bearing deletions for Y-chromosome fertility genes. *Chromosoma.* 83:593–617. <https://doi.org/10.1007/BF00328522>
- Hime, G.R., J.A. Brill, and M.T. Fuller. 1996. Assembly of ring canals in the male germ line from structural components of the contractile ring. *J. Cell Sci.* 109:2779–2788.
- Hoeng, J.C., S.C. Dawson, S.A. House, M.S. Sagolla, J.K. Pham, J.J. Mancuso, J. Löwe, and W.Z. Cande. 2008. High-resolution crystal structure and *in vivo* function of a kinesin-2 homologue in *Giardia intestinalis*. *Mol. Biol. Cell.* 19:3124–3137. <https://doi.org/10.1091/mbc.e07-11-1156>
- Huen, J., Y. Kakihara, F. Ugwu, K.L. Cheung, J. Ortega, and W.A. Houry. 2010. Rvb1-Rvb2: essential ATP-dependent helicases for critical complexes. *Biochem. Cell Biol.* 88:29–40. <https://doi.org/10.1139/O09-122>
- Huizar, R.L., C. Lee, A.A. Boulgakov, A. Horani, F. Tu, E.M. Marcotte, S.L. Brody, and J.B. Wallingford. 2018. A liquid-like organelle at the root of motile ciliopathy. *eLife.* 7:e38497. <https://doi.org/10.7554/eLife.38497>
- Ishikawa, H., and W.F. Marshall. 2011. Ciliogenesis: building the cell's antenna. *Nat. Rev. Mol. Cell Biol.* 12:222–234. <https://doi.org/10.1038/nrm3085>
- Jain, S., J.R. Wheeler, R.W. Walters, A. Agrawal, A. Barsic, and R. Parker. 2016. ATPase-Modulated Stress Granules Contain a Diverse Proteome and Substructure. *Cell.* 164:487–498. <https://doi.org/10.1016/j.cell.2015.12.038>
- Kakihara, Y., and M. Saeki. 2014. The R2TP chaperone complex: its involvement in snoRNP assembly and tumorigenesis. *Biomol. Concepts.* 5: 513–520. <https://doi.org/10.1515/bmc-2014-0028>
- Kee, H.L., J.F. Dishinger, T.L. Blasius, C.J. Liu, B. Margolis, and K.J. Verhey. 2012. A size-exclusion permeability barrier and nucleoporins characterize a ciliary pore complex that regulates transport into cilia. *Nat. Cell Biol.* 14:431–437. <https://doi.org/10.1038/ncb2450>
- Kwitny, S., A.V. Klaus, and G.R. Hunnicutt. 2010. The annulus of the mouse sperm tail is required to establish a membrane diffusion barrier that is engaged during the late steps of spermiogenesis. *Biol. Reprod.* 82: 669–678. <https://doi.org/10.1095/biolreprod.109.079566>
- Lee, C., R.M. Cox, O. Papoulas, A. Horani, K. Drew, C.C. Devitt, S.L. Brody, E.M. Marcotte, and J.B. Wallingford. 2020a. Functional partitioning of a liquid-like organelle during assembly of axonemal dyneins. *bioRxiv*. doi: 10.1101/2020.04.21.052837 (Preprint posted April 21, 2020)
- Lee, C.S., A. Putnam, T. Lu, S. He, J.P.T. Ouyang, and G. Seydoux. 2020b. Recruitment of mRNAs to P granules by condensation with intrinsically-disordered proteins. *eLife.* 9:e52896. <https://doi.org/10.7554/eLife.52896>
- Li, Y., L. Zhao, S. Yuan, J. Zhang, and Z. Sun. 2017. Axonemal dynein assembly requires the R2TP complex component Pontin. *Development.* 144: 4684–4693. <https://doi.org/10.1242/dev.152314>
- Lin, Y.C., P. Niewiadomski, B. Lin, H. Nakamura, S.C. Phua, J. Jiao, A. Levchenko, T. Inoue, R. Rohatgi, and T. Inoue. 2013. Chemically inducible diffusion trap at cilia reveals molecular sieve-like barrier. *Nat. Chem. Biol.* 9:437–443. <https://doi.org/10.1038/nchembio.1252>
- Little, S.C., K.S. Sinsimer, J.J. Lee, E.F. Wieschaus, and E.R. Gavis. 2015. Independent and coordinate trafficking of single *Drosophila* germ plasm mRNAs. *Nat. Cell Biol.* 17:558–568. <https://doi.org/10.1038/ncb3143>
- Liu, G., L. Wang, and J. Pan. 2019. Chlamydomonas WDR92 in association with R2TP-like complex and multiple DNAAFs to regulate ciliary



- dynein preassembly. *J. Mol. Cell Biol.* 11:770–780. <https://doi.org/10.1093/jmcb/mjy067>
- Mao, Y.Q., and W.A. Houry. 2017. The Role of Pontin and Reptin in Cellular Physiology and Cancer Etiology. *Front. Mol. Biosci.* 4:58. <https://doi.org/10.3389/fmolb.2017.00058>
- Medioni, C., K. Mowry, and F. Besse. 2012. Principles and roles of mRNA localization in animal development. *Development.* 139:3263–3276. <https://doi.org/10.1242/dev.078626>
- Müller, H.A.. 2008. Immunolabeling of embryos. *Methods Mol. Biol.* 420: 207–218. [https://doi.org/10.1007/978-1-59745-583-1\\_12](https://doi.org/10.1007/978-1-59745-583-1_12)
- Noguchi, T., M. Koizumi, and S. Hayashi. 2011. Sustained elongation of sperm tail promoted by local remodeling of giant mitochondria in *Drosophila*. *Curr. Biol.* 21:805–814. <https://doi.org/10.1016/j.cub.2011.04.016>
- Olivieri, G., and A. Olivieri. 1965. Autoradiographic study of nucleic acid synthesis during spermatogenesis in *Drosophila melanogaster*. *Mutat. Res.* 2:366–380. [https://doi.org/10.1016/0027-5107\(65\)90072-2](https://doi.org/10.1016/0027-5107(65)90072-2)
- Phillips, D.M.. 1970. Insect sperm: their structure and morphogenesis. *J. Cell Biol.* 44:243–277. <https://doi.org/10.1083/jcb.44.2.243>
- Puchades, C., C.R. Sandate, and G.C. Lander. 2020. The molecular principles governing the activity and functional diversity of AAA+ proteins. *Nat. Rev. Mol. Cell Biol.* 21:43–58. <https://doi.org/10.1038/s41580-019-0183-6>
- Rebollo, E., S. Llamazares, J. Reina, and C. Gonzalez. 2004. Contribution of noncentrosomal microtubules to spindle assembly in *Drosophila* spermatocytes. *PLoS Biol.* 2. E8. <https://doi.org/10.1371/journal.pbio.0020008>
- Reiter, J.F., O.E. Blacque, and M.R. Leroux. 2012. The base of the cilium: roles for transition fibres and the transition zone in ciliary formation, maintenance and compartmentalization. *EMBO Rep.* 13:608–618. <https://doi.org/10.1038/embor.2012.73>
- Riparbelli, M.G., G. Callaini, and T.L. Megraw. 2012. Assembly and persistence of primary cilia in dividing *Drosophila* spermatocytes. *Dev. Cell.* 23:425–432. <https://doi.org/10.1016/j.devcel.2012.05.024>
- Rivera-Calzada, A., M. Pal, H. Munoz-Hernandez, J.R. Luque-Ortega, D. Gil-Carton, G. Degliesposti, J.M. Skehel, C. Prodromou, L.H. Pearl, and O. Llorca. 2017. The Structure of the R2TP Complex Defines a Platform for Recruiting Diverse Client Proteins to the HSP90 Molecular Chaperone System. *Structure.* 25:1145–1152.e1144.
- Robinson, S.W., P. Herzyk, J.A. Dow, and D.P. Leader. 2013. FlyAtlas: database of gene expression in the tissues of *Drosophila melanogaster*. *Nucleic Acids Res.* 41(D1):D744–D750. <https://doi.org/10.1093/nar/gks1141>
- Rosenbaum, J.L., and G.B. Witman. 2002. Intraflagellar transport. *Nat. Rev. Mol. Cell Biol.* 3:813–825. <https://doi.org/10.1038/nrm952>
- Sarpal, R., S.V. Todi, E. Sivan-Loukianova, S. Shirolikar, N. Subramanian, E.C. Raff, J.W. Erickson, K. Ray, and D.F. Eberl. 2003. *Drosophila* KAP interacts with the kinesin II motor subunit KLP64D to assemble chondotonal sensory cilia, but not sperm tails. *Curr. Biol.* 13:1687–1696. <https://doi.org/10.1016/j.cub.2003.09.025>
- Sinden, R.E., E.U. Canning, and B. Spain. 1976. Gametogenesis and fertilization in *Plasmodium yoelii nigeriensis*: a transmission electron microscope study. *Proc. R. Soc. Lond. B Biol. Sci.* 193:55–76. <https://doi.org/10.1098/rspb.1976.0031>
- Sinden, R.E., A. Talman, S.R. Marques, M.N. Wass, and M.J. Sternberg. 2010. The flagellum in malarial parasites. *Curr. Opin. Microbiol.* 13:491–500. <https://doi.org/10.1016/j.mib.2010.05.016>
- Stolc, V., M.P. Samanta, W. Tongprasit, and W.F. Marshall. 2005. Genome-wide transcriptional analysis of flagellar regeneration in *Chlamydomonas reinhardtii* identifies orthologs of ciliary disease genes. *Proc. Natl. Acad. Sci. USA.* 102:3703–3707. <https://doi.org/10.1073/pnas.0408358102>
- Tamma, D., and T.V.S. Tammana. 2017. Human DNA helicase, RuvBL1 and its *Chlamydomonas* homologue, CrRuvBL1 plays an important role in ciliogenesis. *Cytoskeleton (Hoboken).* 74:251–259. <https://doi.org/10.1002/cm.21377>
- Tates, A.D.. 1971. Cytodifferentiation during Spermatogenesis in *Drosophila melanogaster*: An Electron Microscope Study. Vol. Ph.D. Rijksuniversiteit, Leiden.
- Tokuyasu, K.T.. 1975. Dynamics of spermiogenesis in *Drosophila melanogaster*. VI. Significance of “onion” nebenkern formation. *J. Ultrastruct. Res.* 53:93–112. [https://doi.org/10.1016/S0022-5320\(75\)80089-X](https://doi.org/10.1016/S0022-5320(75)80089-X)
- Trcek, T., M. Grosch, A. York, H. Shroff, T. Lionnet, and R. Lehmann. 2015. *Drosophila* germ granules are structured and contain homotypic mRNA clusters. *Nat. Commun.* 6:7962. <https://doi.org/10.1038/ncomms8962>
- Venteicher, A.S., Z. Meng, P.J. Mason, T.D. Veenstra, and S.E. Artandi. 2008. Identification of ATPases pontin and reptin as telomerase components essential for holoenzyme assembly. *Cell.* 132:945–957. <https://doi.org/10.1016/j.cell.2008.01.019>
- Vieillard, J., M. Paschaki, J.L. Duteyrat, C. Augière, E. Cortier, J.A. Lapart, J. Thomas, and B. Durand. 2016. Transition zone assembly and its contribution to axoneme formation in *Drosophila* male germ cells. *J. Cell Biol.* 214:875–889. <https://doi.org/10.1083/jcb.201603086>
- Wang, J.T., J. Smith, B.C. Chen, H. Schmidt, D. Rasoloson, A. Paix, B.G. Lambrus, D. Calidas, E. Betzig, and G. Seydoux. 2014. Regulation of RNA granule dynamics by phosphorylation of serine-rich, intrinsically disordered proteins in *C. elegans*. *eLife.* 3. e04591. <https://doi.org/10.7554/eLife.04591>
- Wang, Y., R. Xu, Y. Cheng, H. Cao, Z. Wang, T. Zhu, J. Jiang, H. Zhang, C. Wang, L. Qi, et al. 2019. RSBP15 interacts with and stabilizes dRSPH3 during sperm axoneme assembly in *Drosophila*. *J. Genet. Genomics.* 46: 281–290. <https://doi.org/10.1016/j.jgg.2019.05.001>
- Wheway, G., L. Nazlamova, and J.T. Hancock. 2018. Signaling through the Primary Cilium. *Front. Cell Dev. Biol.* 6:8. <https://doi.org/10.3389/fcell.2018.00008>
- Yamaguchi, H., T. Oda, M. Kikkawa, and H. Takeda. 2018. Systematic studies of all PIH proteins in zebrafish reveal their distinct roles in axonemal dynein assembly. *eLife.* 7:e36979. <https://doi.org/10.7554/eLife.36979>
- Zhao, L., S. Yuan, Y. Cao, S. Kallakuri, Y. Li, N. Kishimoto, L. DiBella, and Z. Sun. 2013. Reptin/Ruvbl2 is a Lrrc6/Seahorse interactor essential for cilia motility. *Proc. Natl. Acad. Sci. USA.* 110:12697–12702. <https://doi.org/10.1073/pnas.1300968110>
- Zur Lage, P., P. Stefanopoulou, K. Styczynska-Soczka, N. Quinn, G. Mali, A. von Kriegsheim, P. Mill, and A.P. Jarman. 2018. Ciliary dynein motor pre-assembly is regulated by Wdr92 in association with HSP90 co-chaperone, R2TP. *J. Cell Biol.* 217:2583–2598. <https://doi.org/10.1083/jcb.201709026>
- Zur Lage, P., F.G. Newton, and A.P. Jarman. 2019. Survey of the Ciliary Motility Machinery of *Drosophila* Sperm and Ciliated Mechanosensory Neurons Reveals Unexpected Cell-Type Specific Variations: A Model for Motile Ciliopathies. *Front. Genet.* 10:24. <https://doi.org/10.3389/fgene.2019.00024>

Supplemental material

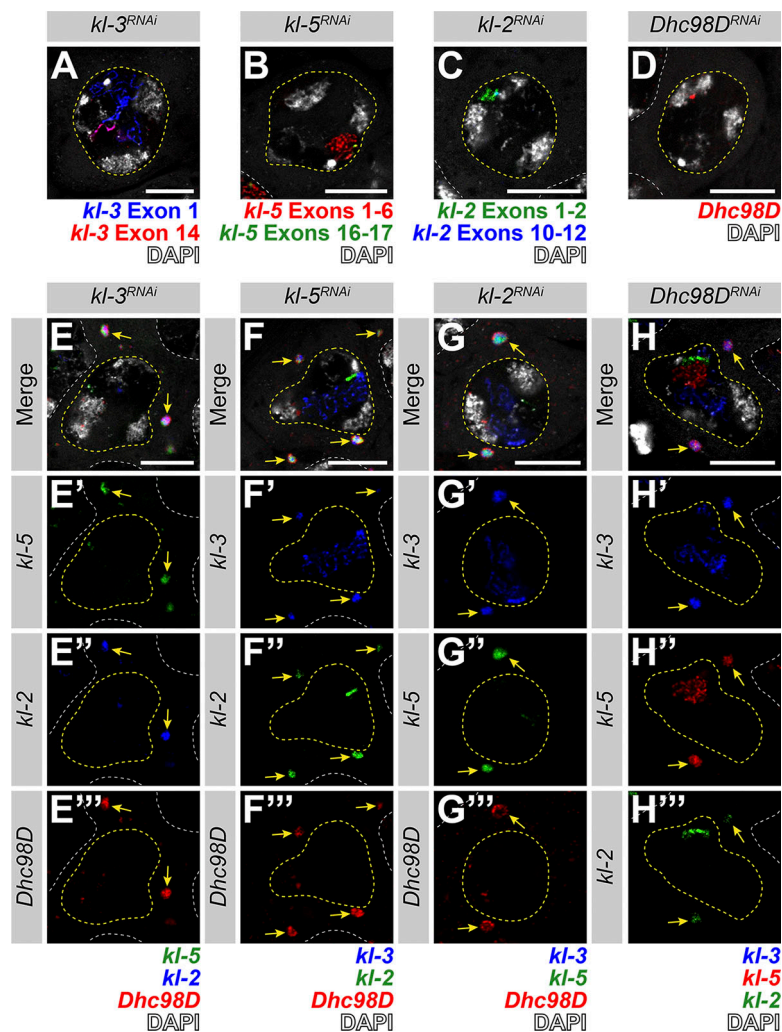


Figure S1. **kl-granule formation is not dependent upon any one mRNA constituent.** (A–D) smFISH against each known kl-granule mRNA constituent following RNAi of that constituent shows successful knockdown (no remaining cytoplasmic signal). Note that we use multiple smFISH probe sets for some mRNAs targeted against different regions of the transcript (see Table S1). (A) *kl-3* exon 1 (blue), *kl-3* exon 14 (red) and DAPI (white). (B) *kl-5* exons 1–6 (red), *kl-5* exons 16–17 (green), and DAPI (white). (C) *kl-2* exons 1–2 (green), *kl-2* exons 10–12 (blue), and DAPI (white). (D) *Dhc98D* (red) and DAPI (white). For all, SC nuclei, yellow dashed line; neighboring SC nuclei, white dashed line. Scale bars: 10 μm. (E–H) smFISH against the other three constituent mRNAs after RNAi of the fourth mRNA. Note that the color used to represent each smFISH probe corresponds to the probe sets in A–D. (E) *kl-5* (green), *kl-2* (blue), *Dhc98D* (red) and DAPI (white). (F) *kl-3* (blue), *kl-5* (green), *Dhc98D* (red), and DAPI (white). (G) *kl-3* (blue), *kl-5* (green), *Dhc98D* (red) and DAPI (white). (H) *kl-3* (blue), *kl-5* (red), *kl-2* (green), and DAPI (white). For all, SC nuclei, yellow dashed line; neighboring SC nuclei, white dashed line; kl-granules, yellow arrows. Scale bars: 10 μm.

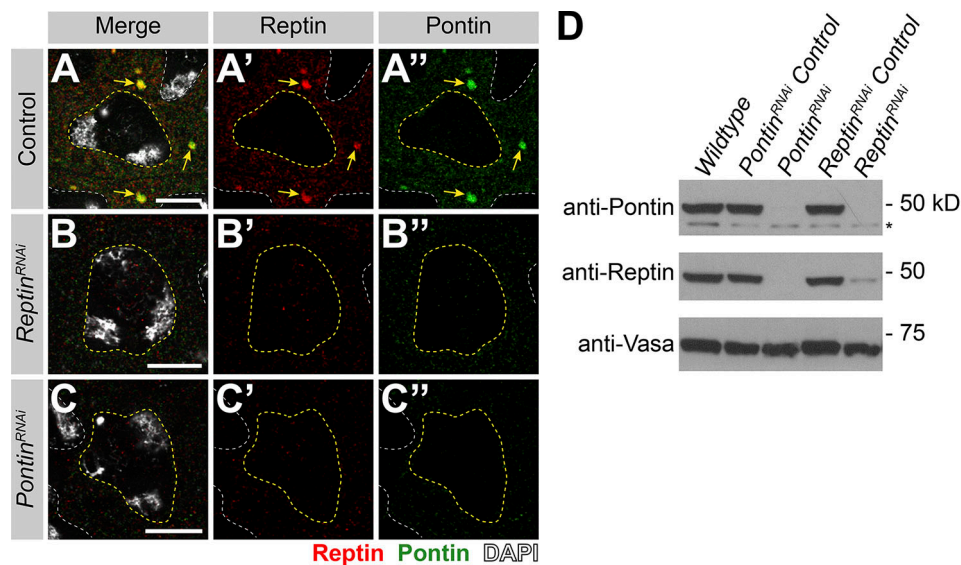


Figure S2. **RNAi of *rept* or *pont* results in loss of both proteins.** (A–C) Rept and Pont protein expression in SCs in control (A), *rept* RNAi (*bam-gal4>UAS-rept<sup>KK105732</sup>*; B), or *pont* RNAi (*bam-gal4>UAS-pont<sup>KK101103</sup>*; C). Shown are Rept (red), Pont (green), DAPI (white), SC nuclei (yellow dashed line), neighboring SC nuclei (white dashed line), and *kl*-granules (yellow arrow). Scale bars: 10  $\mu$ m. (D) Western blot for Pont and Rept in the indicated genotypes. Asterisk indicates nonspecific band.

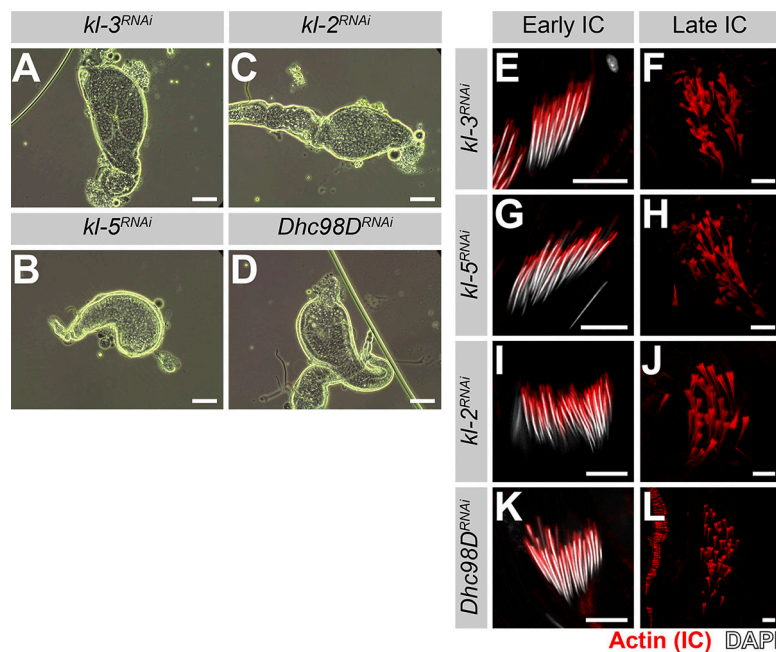


Figure S3. **RNAi of *kl-3*, *kl-5*, *kl-2* or *Dhc98D* results in the same sterility phenotype seen in *rept* or *pont* RNAi testes.** (A–D) Phase-contrast images of seminal vesicles in *kl-3* RNAi (*bam-gal4>UAS-kl-3<sup>TRIP.HMCO3546</sup>*; A), *kl-5* RNAi (*bam-gal4>UAS-kl-5<sup>TRIP.HMCO3747</sup>*; B), *kl-2* RNAi (*bam-gal4>UAS-kl-2<sup>GC8807</sup>*; C) and *Dhc98D* RNAi (*bam-gal4>UAS-Dhc98D<sup>TRIP.HMCO6494</sup>*; D). Bar: 100  $\mu$ m. (E–L) Phalloidin staining of early and late ICs in the indicated genotypes. Phalloidin (Actin, red) and DAPI (white). Bar: 10  $\mu$ m.



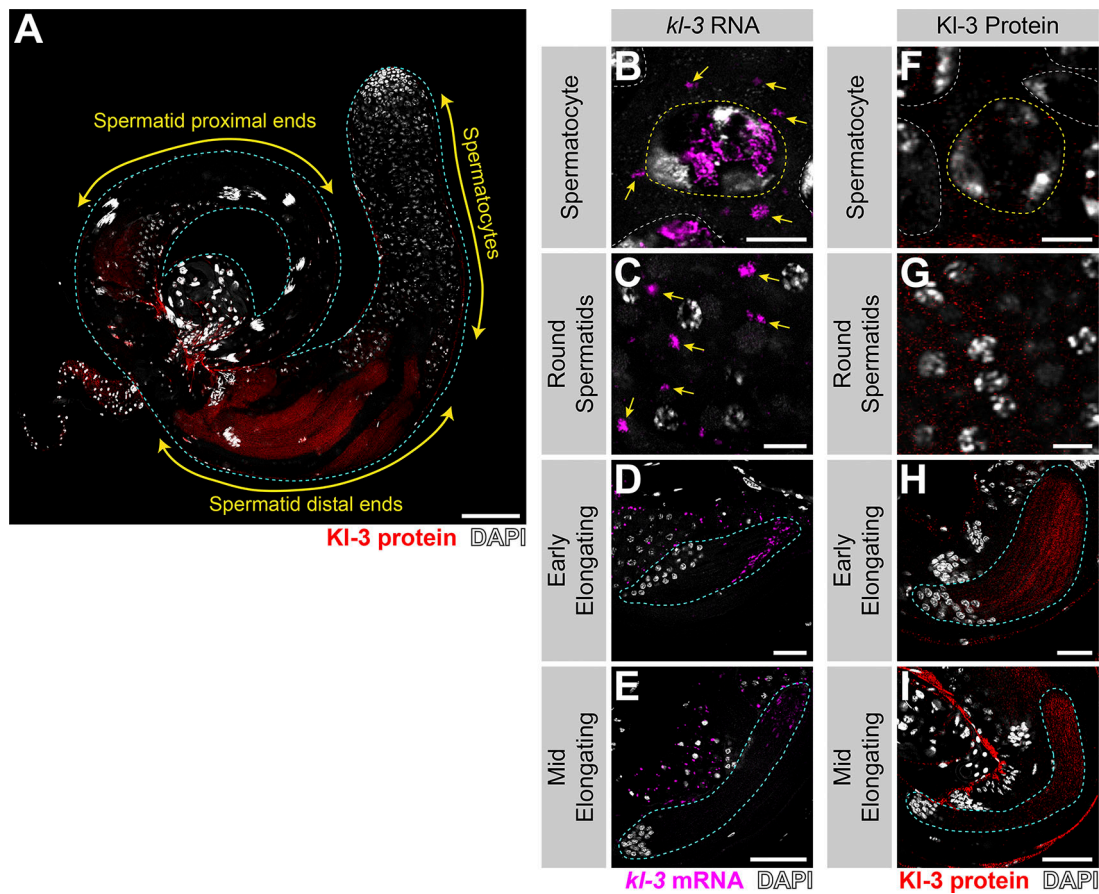
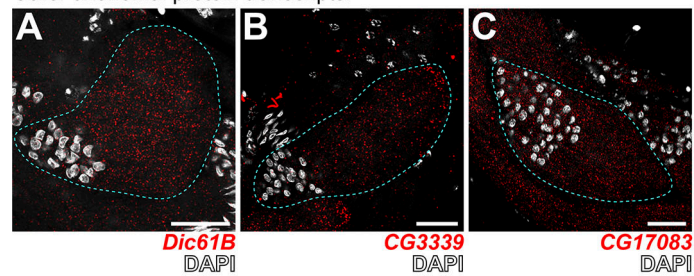
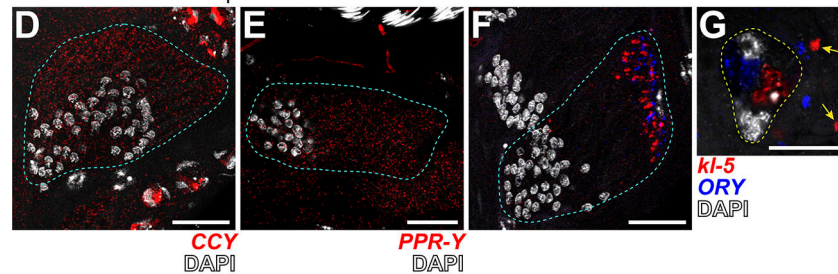


Figure S4. **KL-3 translation correlates with kl-granule dissociation and is enriched at the distal end.** (A) KL-3 3X FLAG protein expression in a wild-type testis. Shown are KL-3 (red), DAPI (white), and testis outline (cyan dashed line). Scale bar: 100  $\mu$ m. (B–E) smFISH for *kl-3* in the indicated developmental stages. Shown are *kl-3* (magenta), DAPI (white), SC nuclei (yellow dashed line), neighboring SC nuclei (white dashed line), a spermatid cyst (cyan dashed line), and kl-granules (yellow arrows). (F–I) KL-3 3X FLAG protein in the indicated developmental stages. Shown are KL-3 (red), DAPI (white), SC nuclei (yellow dashed line), neighboring SC nuclei (white dashed line), and a spermatid cyst (cyan dashed line). Scale bars: 10  $\mu$ m (B, C, F, and G), 25  $\mu$ m (D and H), and 50  $\mu$ m (E and I).

Other axonemal protein transcripts:



Other Y-linked transcripts:



Non-axonemal spermatid protein transcript:

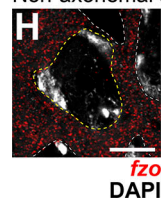


Figure S5. **Transcripts for other axonemal, Y-linked, and spermatid proteins do not localize to kl-granules.** (A–G) smFISH against other axonemal (A–C), Y-linked (D–G), or spermatid-essential (H) transcripts in wild type. (A) *Dic61B* (dynein intermediate chain, red) and DAPI (white). (B) *CG3339* (axonemal dynein heavy chain, red) and DAPI (white). (C) *CG17083* (ODA docking complex, red) and DAPI (white). (D) *CCY* (red) and DAPI (white). (E) *PPR-Y* (red) and DAPI (white). (F and G) *kl-5* (red), *ORY* (blue), DAPI (white), and kl-granules (yellow arrows). (G) *fzo* (red) and DAPI (white). For all, spermatid cyst, cyan; SC nuclei, yellow dashed line; neighboring SC nuclei, white dashed line. Note that because *Fzo* is translated early in spermiogenesis, an SC image was used. Scale bars: 25  $\mu\text{m}$  (A–F) and 10  $\mu\text{m}$  (G and H).

Table S1 is provided online and shows smFISH probes and quantitative RT-PCR primers used in this study.